The Meteoritical Society

Meteoritics & Planetary Science 42, Nr 9, 1529–1548 (2007)
Abstract available online at http://meteoritics.org

Numerical simulations of the differentiation of accreting planetesimals with ^{26}Al and ^{60}Fe as the heat sources

S. SAHIJPAL*, P. SONI, and G. GUPTA

Department of Physics, Panjab University, Chandigarh, India 160 014
*Correponding author. E-mail: sandeep@pu.ac.in

(Received 26 February 2006; revision accepted 24 February 2007)

Abstract–Numerical simulations have been performed for the differentiation of planetesimals undergoing linear accretion growth with ^{26}Al and ^{60}Fe as the heat sources. Planetesimal accretion was started at chosen times up to 3 Ma after Ca-Al-rich inclusions (CAIs) were formed, and was continued for periods of 0.001–1 Ma. The planetesimals were initially porous, unconsolidated bodies at 250 K, but became sintered at around 700 K, ending up as compact bodies whose final radii were 20, 50, 100, or 270 km. With further heating, the planetesimals underwent melting and igneous differentiation. Two approaches to core segregation were tried. In the first, labelled A, the core grew gradually before silicate began to melt, and in the second, labelled B, the core segregated once the silicate had become 40% molten. In A, when the silicate had become 20% molten, the basaltic melt fraction began migrating upward to the surface, carrying ^{26}Al with it. The ^{60}Fe partitioned between core and mantle. The results show that the rate and timing of core and crust formation depend mainly on the time after CAIs when planetesimal accretion started. They imply significant melting where accretion was complete before 2 Ma, and a little melting in the deep interiors of planetesimals that accreted as late as 3 Ma. The latest melting would have occurred at <10 Ma. The effect on core and crust formation of the planetesimal's final size, the duration of accretion, and the choice of $(^{60}Fe/^{56}Fe)_{initial}$ were also found to be important, particularly where accretion was late. The results are consistent with the isotopic ages of differentiated meteorites, and they suggest that the accretion of chondritic parent bodies began more than 2 or 3 Ma after CAIs.

INTRODUCTION

The differentiation of planetesimals in the early solar system resulted in a wide range of differentiated meteorite parent bodies (Taylor et al. 1993; Hewins and Newsom 1988; Haack and McCoy 2004; Chabot and Haack 2006; McCoy et al. 2006). Based on the ^{182}Hf-^{182}W systematic in iron meteorites, the core differentiation of planetesimals occurred within the initial few million years during the formation of the solar system (Horan et al. 1998; Kleine et al. 2002; Yin et al. 2002; Kleine et al. 2005a, 2005b; Markowski et al. 2006; Scherstén et al. 2006; Qin et al. 2006; Bottke et al., 2006). There are indications of protracted core differentiation in rare cases (e.g., Dauphas et al. 2005). The ^{182}Hf-^{182}W systematic in the majority cases indicate rapid accretion growth and core-mantle differentiation of the parent bodies of iron meteorites over time scales comparable to that inferred from the Ca-Al-rich inclusions and chondrules (Bizzarro et al. 2004, 2005, 2006a). Evidence for the crust-mantle differentiation of planetesimals within the initial few million years comes from the ^{26}Al-^{26}Mg and ^{53}Mn-^{53}Cr systematics in eucrites and angrites (Srinivasan et al. 1999; Srinivasan 2002; Nyquist et al. 2001, 2003a, 2003b, 2003c; Baker et al. 2005; Bizzarro et al. 2005; Markowski et al. 2006).

The rapid differentiation and small sizes of planetesimals in the early solar system necessitate a potent heat source that could provide the adequate thermal energy to the planetesimals against the heat conduction losses (e.g., Wood and Pellas 1991; McSween et al. 2002; Chabot and Haack 2006; McCoy et al. 2006). The radiogenic decay energy of the short-lived nuclide ^{26}Al has been proposed as a plausible heat source (Urey 1955). The widespread presence of ^{26}Al in the early solar system has been established in Ca-Al-rich inclusions (CAIs) and chondrules (e.g., MacPherson et al. 1995; Bizzarro et al. 2004), and the short-lived nuclide could have provided the heat for the differentiation and thermal metamorphism of planetesimals. Alternatively, viable heat sources include impact energy released during the accretion of planetesimals and the electromagnetic induction heating of the planetesimals moving around the magnetically active protosun (Sonett et al. 1968). The recent laboratory experiments indicate that the induction heating alone cannot explain the thermal processing of planetesimals (Marsh et al. 2006), whereas the impact energy can only cause localized heating and melting of a planetesimal without their fragmentation (Keil et al. 1997). The decline in the role played by the impact and the induction heating favors the radiogenic decay energy of short-lived nuclei as the primary heat source for differentiation of planetesimals. The recently revised estimates of the $(^{60}Fe/^{56}Fe)_{initial}$ ratio in the early solar system (Mostefaoui et al. 2004, 2005; Tachibana and Huss 2003) suggest that the initial solar abundance of ^{60}Fe along with ^{26}Al could have provided the necessary thermal energy for differentiation. The present work deals with the detailed numerical simulations of the differentiation of planetesimals undergoing accretion with ^{26}Al and ^{60}Fe as the heat source.

Several groups have developed a wide range of thermal models of planetesimals with ^{26}Al as the heat source (Miyamoto et al. 1981; Miyamoto 1991; Grimm and McSween 1993; Sahijpal et al. 1995; Bennett and McSween 1996; Sahijpal 1997; Ghosh and McSween 1998, 1999; Ghosh et al. 2003; Merk et al. 2002; Yoshino et al. 2003; Sahijpal and Soni 2005; Bizzarro et al. 2005; Hevey and Sanders 2006; Sahijpal 2006). The main motivation behind these studies is to develop realistic thermal models for differentiation or thermal metamorphism. Most of the earlier thermal models deal with the thermal metamorphism of meteorite parent bodies. Ghosh and McSween (1998) developed the first comprehensive model of the differentiation of a planetesimal with ^{26}Al as the heat source. This model provides the benchmark to quantitatively understand the differentiation processes. Merk et al. (2002) developed a thermal model of a planetesimal undergoing a linear accretion growth with ^{26}Al as the heat source. However, the differentiation processes were not incorporated in this model. Bizzarro et al. (2005) have recently developed thermal models of the heating of asteroids using ^{26}Al and ^{60}Fe as the heat sources. In addition, the recent thermal models by Hevey and Sanders (2006) incorporate thermal convection in a molten planetesimal that was accreted instantaneously.

In the present work, we have made an attempt to develop realistic differentiation models that incorporate some of the physical processes involved in the planetary accretion and the subsequent differentiation of asteroids (Taylor et al. 1993; Haack and McCoy 2004; Chabot and Haack 2006; McCoy et al. 2006). We have performed comprehensive numerical simulations of the differentiation of planetesimals of final radii 20–270 km with ^{26}Al and ^{60}Fe as the heat source. The planetesimals with radii of a few tens of kilometers are usually considered to be the source of iron meteorites (Chabot and Haack 2006), whereas the larger bodies, e.g., the asteroid 4 Vesta with a radius of ~270 km, are the potential sources of howardite-eucrite-diogenite (HED) meteorites (Ghosh and McSween 1998). However, Yang et al. (2006) have recently suggested that the IVA iron meteorites could have been derived from a metal core 300 km across that had lost its mantle. Compared to the instantaneous planetary accretion models (Ghosh and McSween 1998; Bizzarro et al. 2005; Hevey and Sanders 2006), we have considered a linear accretion growth of the planetesimals over the time scales of 0.001–1 million years to understand its influence on the thermal evolution of planetesimals. We have numerically simulated for the first time the gradual growth of the iron core due to the inward flow of Fe-FeS melt towards the center of the planetesimals. This is distinct from the previous model (Ghosh and McSween 1998), which instantaneously triggers the core and the crust formation of a planetesimal. In addition, subsequent to the initiation of silicate melting, the outward extrusion of the basaltic melt to form a crust has been parametrically modeled for a specific melt percolation velocity. Finally, in contrast to the recent differentiation models with a fixed insulating regolith thickness (Sahijpal and Soni 2005; Sahijpal 2006), we have now considered the sintering and the volume loss of the bulk body at ~700 K (Hevey and Sanders 2006). One of the major objectives of developing a detailed thermal model for differentiation is to study the dependence of the growth rate of Fe-FeS core on the onset time of the planetesimal accretion, the accretion rate, the size of the planetesimal, and the $(^{60}Fe/^{56}Fe)_{initial}$ ratio. In addition, we want to deduce temporal scales involved in the differentiation processes in the early solar system in case ^{26}Al and ^{60}Fe were the exclusive planetary heat sources. Furthermore, these temporal scales have to be examined in context with the increasingly precise chronological data available from differentiated meteorites.

METHODOLOGY

Heat Conduction Equation

The heat conduction partial differential equation for a spherically symmetric planetesimal with uniformly distributed ^{26}Al and ^{60}Fe (Table 1) was solved using the finite difference method with the classic explicit approximation (Lapidus and Pinder 1982). The temporal grid (Tgrid) and the spatial grid (Sgrid) sizes of 1 yr and 300 m, respectively, were chosen to obtain the required consistency and stability in the numerical solutions (Lapidus and Pinder 1982). In addition, we preferred the above specific choices to numerically facilitate the various physical processes that include the accretion of the planetesimals, the sintering, and the differentiation. A constant surface temperature of 250 K (Hevey and Sanders 2006) corresponding to the solar nebula ambient temperature was maintained for the planetesimals. In the case of an instantaneously accreted planetesimal (Sahijpal et al. 1995; Sahijpal 1997), the solutions obtained from the

Table 1. The adopted values of the various simulation parameters.

	Simulation parameter	Adopted value
1	Radii of planetesimals subsequent to sintering	20, 50, 100, 270 km
2	Accretion duration	0.001–1 Ma
3	Spatial grid size of simulations	300 m
4	Temporal grid size of simulations	1 yr
5	Decay energy of ^{26}Al	3.16 MeV (Ferguson 1958; Schramm et al. 1970)
6	Decay energy of ^{60}Fe	3 MeV
7	Mass abundance of Al	1.22% (Dodd 1981)
8	Mass abundance of Fe	27.8% (Dodd 1981)
9	Canonical value of $(^{26}Al/^{27}Al)_{initial}$	5×10^{-5} (MacPherson et al. 1995)
10	Initial value of $^{60}Fe/^{56}Fe$ at the time of formation of CAIs with canonical value of $(^{26}Al/^{27}Al)_{initial}$	$(0–2) \times 10^{-6}$
11	Initial ^{26}Al power per unit mass of undifferentiated planetesimals	2.2×10^{-7} W kg^{-1}
12	Initial ^{60}Fe power per unit mass of undifferentiated planetesimal for $(^{60}Fe/^{56}Fe)_{initial} = (0.5–2) \times 10^{-6}$	$(1.01\text{-}3.96) \times 10^{-8}$ W kg^{-1}
13	Density of the sintered planetesimals	3560 kg m^{-3} (Yomogida and Matsui 1983)
14	Density of Fe-FeS core	7800 kg m^{-3}
15	Ambient temperature	250 K (Hevey and Sanders 2006)
16	Sintering temperature	670–700 K
17	Thermal diffusivity of unsintered planetesimal (κ)	6.4×10^{-10} m^2 s^{-1} in the range 250–670 K
18	Thermal diffusivity of sintered planetesimal (κ)	$(6.4–5.4) \times 10^{-7}$ m^2 s^{-1} in the range 700–1450 K (Yomogida and Matsui 1983)
19	Thermal diffusivity of molten Fe-FeS	5×10^{-6} m^2 s^{-1} for B simulations 5×10^{-4} m^2 s^{-1} for A simulations (In order to thermally imitate convection)
20	Specific heat of the unmelted silicate	610–830 J kg^{-1} K^{-1} in the range 250–1450 K (Ghosh and McSween 1999)
21	Specific heat of silicate and Fe-FeS melts	2000 J kg^{-1} K^{-1} (Ghosh and McSween 1998)
22	The solidus and the liquidus of the Fe-FeS	1213–1233 K (Ghosh and McSween 1998)
23	The solidus and the liquidus of the silicate	1450–1850 K (Taylor et al. 1993)
24	Latent heat of Fe-FeS melting	2.7×10^5 J kg^{-1} (Ghosh and McSween 1998)
25	Latent heat of silicate melting	4.0×10^5 J kg^{-1} (Ghosh and McSween 1998)

finite difference method were found to be consistent with the analytical solutions of the partial differential equation (Hevey and Sanders 2006) solved using the temperature independent specific heat and thermal diffusivity (κ, m^2 s^{-1}). Finally, we made comparisons of our simulation results with those obtained recently by several other groups (Ghosh and McSween 1998, 1999; Ghosh et al. 2003; Bizzarro et al. 2005; Hevey and Sanders 2006). These specific simulations were run with the simulation parameters identical to the one chosen by the various groups. It should be noted that the finite element method along with the radiation boundary condition used by Ghosh and McSween (1998) is more robust compared to the finite difference method for the partial differential equation with the fixed boundary condition employed in the present work.

Accretion Growth of the Planetesimals

We have considered a linear rate of increase in radius of the planetesimals (Merk et al. 2002), $R(t) = R_o + \alpha t$, where R_o is the initial radius and $R(t)$ is the radius of the planetesimal at a specific time t. If R_{max} is the maximum radius attained by the planetesimal in time $t_{duration}$, then $\alpha = (R_{max} - R_o)/t_{duration}$. We have performed simulations for the planetesimal radii of 26, 65, 130, and 351 km. Subsequent to sintering, these planetesimals will finally acquire radii of 20, 50, 100, and 270 km, respectively. We adopted the latter values throughout the text to represent the final radius of the planetesimal. The accretion growth of the porous (unconsolidated) bodies were set out with an R_o = 300 m sized planetary embryo at a time interval t_{onset} Ma after the formation of the CAIs with the canonical value of 5×10^{-5} for the $^{26}Al/^{27}Al$ ratio (MacPherson et al. 1995). The accretion growth of the planetesimal was performed by modifying the spatial grid array of the finite difference code without altering the spatial grid size. According to the accretion rate, a spatial grid unit of size 300 m was appended at a specific time to the pre-existing spatial grid array representing the planetesimal, thereby resulting in the gradual growth of the planetesimal in an incremental size step of 300 m. During the growth, the average temperature of the bodies 300 m in size accreting on the planetesimal was assumed to be identical to the ambient temperature (~250 K, in the present work) of the solar nebula (Ghosh et al. 2003). It is unlikely that a body 300 m in size will attain higher temperature due to the radioactive decay. We employed the moving boundary condition for the accretion growth of the planetesimals by redefining the planetesimal surface each time the spatial grid array was enlarged. A constant surface temperature of 250 K was maintained on the gradually growing spatial grid array.

The simulations were mostly carried out with t_{onset} in the range of 0–3.6 Ma, with t_{onset} = 0 Ma corresponding to the initiation of the planetesimal accretion at the time of the condensation of CAIs with the canonical value of 5×10^{-5} for $^{26}Al/^{27}Al$. A couple of simulations were carried out for t_{onset} = –0.35 Ma. This corresponds to the initiation of the planetesimal accretion at the time of the condensation of the CAI with the supracanonical $^{26}Al/^{27}Al$ ratio (Young et al. 2005). Due to the uncertainty in defining the $(^{60}Fe/^{56}Fe)_{initial}$ ratio in the early solar system (Mostefaoui et al. 2004, 2005; Tachibana and Huss 2003), we carried out most of the numerical simulations in the range of $(0.5–2) \times 10^{-6}$ for the $(^{60}Fe/^{56}Fe)_{initial}$ ratio at the time of the formation of the CAIs with the canonical value of 5×10^{-5} for $^{26}Al/^{27}Al$. We have also explored the feasibility of the accretion and differentiation of planetesimals prior to the injection of ^{60}Fe in the early solar system by running some simulations exclusively with ^{26}Al decay energy (Bizzarro et al. 2006b). Nickel isotopic analyses of the various meteorites and meteoritic phases by Bizzarro et al. (2006b) indicate the possibility of the late injection of ^{60}Fe into the early solar system where ^{26}Al was already widespread.

Subsequent to the initiation of the accretion, a planetesimal gradually attained its final radius over a specific time span $t_{duration}$ (Ma). We carried out simulations for $t_{duration}$ in the range of 0.001–1 Ma. The lower time interval corresponds to almost instantaneous growth. In these sets of simulations, the initial differences in the temperatures at the center and near the surface of the finally accreted planetesimals were found to be a few degrees, thereby confirming their almost instantaneous growth. The upper time duration of the accretion corresponds to the accretion growth of the median-sized planetesimals over a theoretical time span of a few million years (Weidenschilling 1988; Ghosh et al. 2003). The various parameters chosen for the simulations are presented in Table 1.

The H-chondrite composition was chosen for the planetesimals for simplification. The compositions of the ordinary chondrites (Dodd 1981; Jarosewich 1990) are the most suitable for developing thermal models of differentiation, as the melting of these chondrites can be well understood both theoretically and experimentally (see e.g., Taylor et al. 1993; McCoy et al. 2006). However, it should be noted that several groups of iron meteorites have precursor compositions distinct from ordinary chondrites. The H-chondrite composition would probably serve as a precursor composition of the HED bodies. The H-chondrite abundances of 1.22% and 27.8% were assumed for the uniformly distributed Al and Fe, respectively, in the undifferentiated planetesimals (Dodd 1981).

Sintering of the Planetesimals

Hevey and Sanders (2006) have recently considered the influence of sintering and planetary volume loss at ~700 K for an instantaneously accreted planetesimal. We followed an identical approach for the planetesimal undergoing accretion growth. This is an improvement over our recent differentiation models that deal with a fixed sized insulating regolith (Sahijpal and Soni 2005; Sahijpal 2006). In the present work, the growth of the planetesimals was assumed to commence from porous (unconsolidated) nebular dust of ~55% porosity. The thermal diffusivity (κ, $m^2 s^{-1}$) of the unconsolidated body was assumed to be three orders of magnitude lower than that of the heated consolidated body (Yomogida and Matsui 1983). We have considered the sintering of the planetesimals in the assumed temperature range of 670–700 K. Within this temperature range, the thermal diffusivity was increased steadily by three orders of magnitude at an assumed rate of one order of magnitude increase per 10 K. The porosity of the body was reduced to a final porosity of zero within this temperature range on account of compaction (planetary volume loss). The spatial grid array was deformed due to the shrinking of the planetesimal on account of sintering. A planetesimal 100 km in radius will initiate with the accretion of an unconsolidated body ~130 km in size (Hevey and Sanders 2006). Subsequent to sintering, a sharp thermal gradient within less than 10 km of the planetesimal surface was observed in most of the simulations. The thermal gradient becomes extreme over the outermost spatial grids owing to a constant surface temperature of 250 K. In general, the entire planetesimal experienced complete sintering in most of the simulations except for the spatial grids representing the outer ~1.8 km (6 spatial grids) and ~0.9 km (3 spatial grids) for the simulations with $t_{duration}$ of 1 Ma and ≤0.1 Ma, respectively. The outer spatial grids were partially sintered and provided a thin insulating regolith to the planetesimal for the subsequent thermal evolution. It should be noted that during the extrusion of the basaltic melt to the surface, the nature of the surface regolith would drastically change. This would influence its thermal insulation provided to the inner regions, hence the cooling rate of the planetesimal. We have considered the influence of the melt extrusion through the planetesimal surface regolith. Subsequent to the extrusion of the basaltic melt the entire planetesimal experienced complete sintering with no insulating regolith to provide additional thermal blanket.

In order to consider the temperature dependence of the specific heat and the thermal diffusivity (κ, $m^2 s^{-1}$) subsequent to the sintering, we followed an identical approach as chosen by Sahijpal (1997), and Ghosh and McSween (1999). The temperature dependence of the thermal diffusivity (Yomogida and Matsui 1983) and the specific heat (Ghosh and McSween 1999) were used in the simulations. To avoid any discontinuity in temperature and other thermal properties during sintering and at the regolith surface, the thermal diffusivity at a specific spatial grid was estimated by averaging its value with the thermal diffusivities of the two nearest-neighboring spatial grids. This approach resulted in a gradual fall of the temperature from ~700 K to 250 K near the regolithic surface of the planetesimal. We monitored the variations in the several thermal parameters and observed no instability in the solutions. The thermal diffusivity of the molten Fe-FeS was assumed to be 5×10^{-6} m^2 s^{-1}. However, in order to thermally imitate the influence of convection in the molten Fe-FeS core, we considered three orders of magnitude high thermal diffusivity of 5×10^{-4} m^2 s^{-1} compared to the thermal diffusivity of the sintered rock (Table 1).

Planetary Differentiation

The differentiation of a planetesimal involves segregation of $(\text{Fe-Ni})_{\text{metal}}$-FeS melt from the bulk chondrite to form an iron sulfide core and a silicate mantle (Taylor et al. 1993; Hewins and Newsom 1988; Haack and McCoy 2004; McCoy et al. 2006). The partial melting of silicate can result in the production of a melt of basaltic composition that can ascent upward due to its lower density compared to the adjoining rock (Taylor et al. 1993; McCoy et al. 2006). A large-scale silicate melting can result in the production of a magma ocean (Taylor et al. 1993). In the present work, we have numerically modeled the descent of the $(\text{Fe-Ni})_{\text{metal}}$-FeS melt toward the center of the planetesimal to form a core. In addition, we have parametrically modeled the ascent of the basaltic melt for a specific melt percolation velocity.

Even though the numerical modeling of the differentiation processes can be performed to a reasonable accuracy, the uncertainties involved in the physics of the segregation of $(\text{Fe-Ni})_{\text{metal}}$-FeS melt from the bulk chondrite by porous flow pose major difficulty for developing a robust differentiation model. Distinct scenarios have been proposed for the segregation (Taylor 1992; Taylor et al. 1993; Ghosh and McSween 1998). These include the segregation of the $(\text{Fe-Ni})_{\text{metal}}$-FeS melt from the bulk chondrite in the temperature range of 1450–1850 K (the assumed solidus and liquidus of the silicate) once the silicate melt fraction exceeds ~0.4 (Taylor 1992; Taylor et al. 1993). The alternative scenario involves the initiation of the melt segregation at comparatively lower temperatures (1213–1233 K, the assumed solidus and liquidus of the Fe-FeS, respectively) before significant melting of the bulk chondrite (e.g., Ghosh and McSween 1998). This scenario is based on the observation of $(\text{Fe-Ni})_{\text{metal}}$-FeS veins in the acapulcoite (e.g., McCoy et al. 1996). However, it is quite likely that in the absence of substantial silicate melting these veins would not result in the large-scale segregation of iron sulfide to form a core (Taylor et al. 1993; Ghosh and McSween 1998; McCoy et al. 1996, 2006). Ghosh and McSween (1998) have presented a wide range of differentiation scenarios due to the uncertainties in the temporal sequence of core formation with respect to silicate melting and the crust differentiation. Some of these scenarios deal with the core formation prior to silicate melting, whereas in other cases the core formation commenced subsequent to silicate melting. The formation of the crust subsequent to silicate melting has been proposed in some of these scenarios. We have simulated two of these distinct differentiation scenarios in the present work. These include:

- The set of simulations (labelled A) where the initiation of the segregation of $(\text{Fe-Ni})_{\text{metal}}$-FeS melt occurred at 1213–1233 K prior to silicate melting. This was followed by silicate melting at higher temperatures and the extrusion of the basaltic melt to the planetesimal surface, and
- The set of simulations (labelled B) where the initiation of the segregation of $(\text{Fe-Ni})_{\text{metal}}$-FeS melt commences once the silicate melt fraction exceeds ~0.4. Subsequent to silicate melting, the basaltic melt was not removed from its source region in this set of simulations.

It should be emphasized that so far we have been able to successfully simulate only these two sets of differentiation scenarios. The remaining possible scenarios (e.g., Ghosh and McSween 1998) that could be equally feasible are beyond the scope of the present work.

A Simulations

In the A set of simulations, we considered the melting and the segregation of the entire FeS contents of the bulk H chondrite (Dodd 1981; Jarosewich 1990) to commence within 1213–1233 K. This was accompanied by varying proportions of $(\text{Fe + Ni})_{\text{metal}}$ segregation. We have performed simulations with two different extents of $(\text{Fe-Ni})_{\text{metal}}$ segregation. In most of the simulations, the entire Fe_{metal} and Ni_{metal} contents of the bulk chondrite (Jarosewich 1990), i.e., 16% and 1%, respectively, were segregated along with the entire FeS (Fe = 3% and S = 2%) to form an (FeS + Fe[16%]) core. In an alternative set of simulations, $(\text{Fe-Ni})_{\text{metal}}$ ~2% (Fe = 2%; Ni = 0.13%) of the bulk chondrite was segregated along with the entire FeS to form an (FeS + Fe[2%]) core. The remaining $(\text{Fe-Ni})_{\text{metal}}$ contents were retained by the silicate matrix until it melted. This scenario would be identical to the differentiation scenario proposed for the IID iron meteorites by Wasson and Huber (2006). It should be mentioned that in order to explain the sulfur depletion in several groups of iron meteorites, e.g., IIIAB, IVA, and IVB groups, the partial loss of Fe-FeS by explosive volcanism has been suggested as a viable mechanism (Keil and Wilson 1993; McCoy et al. 2006). Alternatively, the parent bodies of the sulfur-depleted iron meteorites could have accreted from material that was distinct from the chondrites studied so far. If feasible, the explosive volcanism will be prominent in small planetesimals of radii of a few tens of kilometers. It is quite likely that during their initial accretion stages and melting, these

Table 2. The growth of the Fe + FeS core and the initiation of the basaltic melt extrusion for the differentiation of planetesimals undergoing a linear rate of increase in radius.

No.	Simulations[a]	Figure reference	Fe-FeS core[b]					Basaltic melt extrusion[c]
	Radius: 20 km		0+ km	2 km	4 km	6 km	8 km	
1	A20-(-0.35)-0.001-0(0)	–	–0.266	–0.265	–0.265	–0.265	–0.263	–0.241
2	A20-0-0.001-0(0)	–	0.120	0.120	0.120	0.120	0.126	0.156
3	A20-0-0.001-0(0)-3	–	0.126	0.126	0.129	0.129	0.135	0.165
4	A20-0-0.001-0(0)-4	–	0.093	0.093	0.096	0.096	0.096	0.123
5	A20-0-0.001-1(-6)	–	0.108	0.108	0.108	0.108	0.113	0.143
6	A20-0-0.001-2(-6)	–	0.098	0.098	0.098	0.098	0.102	0.132
7	A20-0.5-0.001-1(-6)	2a	0.680	0.680	0.680	0.680	0.695	0.740
8	A20-0.5-0.001-2(-6)-30	–	0.655	0.655	0.655	0.655	0.665	0.725
9	A20-1-0.001-2(-6)	–	1.243	1.243	1.243	1.245	1.284	1.339
10	B20-1-0.001-2(-6)	–	1.420	1.420	1.420	1.428	2.000	1.338
11	A20-2-0.001-5(-7)	–	3.008	3.008	3.020	3.134	none	4.144
12	A20-2-0.001-1(-6)	–	2.827	2.827	2.831	2.878	none	3.406
13	A20-2-0.001-1(-6)-3	–	2.878	2.878	2.885	2.938	none	3.560
14	A20-2-0.001-1(-6)-4	–	2.645	2.645	2.645	2.660	none	2.975
15	A20-2-0.001-2(-6)	2b	2.621	2.621	2.621	2.635	none	2.992
16	B20-2-0.001-2(-6)	2c	3.208	3.215	3.305	none	none	2.923
17	A20-2-0.001-2(-6)-2%	–	2.620	2.620	2.633	–	–	2.940
18	A20-2-0.1-1(-6)	–	2.883	2.883	2.944	3.035	none	3.613
19	A20-2-0.1-2(-6)	–	2.660	2.660	2.700	2.761	none	3.126
20	A20-3-0.001-2(-6)	–	4.862	4.880	5.067	none	none	none
	Radius: 50 km		0+ km	5 km	10 km	15 km	20 km	
1	A50-(-0.35)-0.5-0(0)	–	–0.25	–0.15	–0.04	0.07	0.18	–0.21
2	A50-0-0.1-0(0)	–	0.13	0.14	0.17	0.19	0.23	0.19
3	A50-0.5-0.001-2(-6)	–	0.65	0.65	0.65	0.65	0.65	0.71
4	A50-1-0.001-2(-6)	–	1.24	1.24	1.24	1.25	1.25	1.33
5	A50-2-0.001-2(-6)	2d	2.62	2.62	2.62	2.62	2.66	2.98
6	A50-2-0.01-2(-6)	–	2.62	2.62	2.63	2.63	2.70	2.99
7	A50-2-0.1-1(-6)	–	2.84	2.87	2.93	2.96	3.24	3.51
8	A50-2-0.1-2(-6)	2e	2.63	2.66	2.69	2.72	2.81	3.09
9	A50-2-1-1(-6)	–	2.99	3.27	3.86	4.64	none	none
10	A50-2-1-2(-6)	2f	2.72	2.96	3.39	3.93	none	3.81
11	B50-2-1-2(-6)	–	3.39	3.69	4.23	5.56	none	3.03
12	A50-2-1-2(-6)-2%	–	2.72	3.21	–	–	–	3.33
13	A50-2.9-0.1-1(-6)	2g	7.15	7.30	7.97	none	none	none
14	A50-3-0.1-2(-6)	2h	4.90	4.93	5.02	5.11	none	none
	Radius: 100 km		0+ km	10 km	20 km	30 km	40 km	
1	A100-0.5-1-2(-6)	–	0.68	0.92	1.16	1.40	1.70	0.77
2	A100-0.5-1-2(-6)-30	–	0.68	0.92	1.16	1.40	1.67	0.83
3	A100-1-1-1(-6)	2i	1.33	1.57	1.87	2.20	2.56	1.54
4	A100-1-1-2(-6)	–	1.27	1.51	1.81	2.05	2.38	1.48
5	A100-2-0.1-1(-6)	–	2.84	2.87	2.93	2.96	3.02	3.50
6	A100-2-0.1-2(-6)	–	2.63	2.66	2.69	2.74	2.77	3.08
7	B100-2-0.1-2(-6)	–	3.23	3.26	3.32	3.38	3.47	2.93
8	A100-2-0.001-2(-6)	–	2.62	2.62	2.62	2.62	2.62	2.98
9	A100-2-1-5(-7)	2j	3.11	3.62	4.53	7.00	none	none
10	A100-2-1-1(-6)	2k	2.93	3.29	3.93	4.69	none	4.29
11	A100-2-1-2(-6)	2l	2.69	3.02	3.38	3.83	4.44	3.65
12	B100-2-1-2(-6)	2m	3.29	3.65	4.34	5.48	none	3.00
13	A100-3-1-2(-6)	2n	5.08	5.77	7.15	none	none	none
14	A100-2-1-2(-6)-2%	–	2.69	3.20	–	–	–	3.20

Table 2. *Continued.* The growth of the Fe + FeS core and the initiation of the basaltic melt extrusion for the differentiation of planetesimals undergoing a linear rate of increase in radius.

No.	Simulations[a]	Figure reference	Fe-FeS core[b]					Basaltic melt extrusion[c]
	Radius: 270 km		0+ km	27 km	54 km	81 km	108 km	
1	A270-0.5-1-1(-6)	–	0.72	0.94	1.22	1.45	1.72	0.83
2	A270-0.5-1-2(-6)	–	0.67	0.90	1.15	1.41	1.68	0.79
3	A270-1-1-2(-6)	–	1.26	1.51	1.80	2.06	2.42	1.44
4	A270-2-1-1(-6)	2o	2.87	3.31	3.89	4.71	6.22	4.87
5	A270-2-1-2(-6)	–	2.65	2.98	3.41	3.83	4.45	3.58
6	A270-3-1-2(-6)	2p	4.93	5.74	7.16	none	none	none

[a]The simulations are titled according the choice of the various parameters. These parameters are separated by hyphens. In order these parameters are: i) The simulation type (A or B) and the radius of the planetesimals subsequent to complete sintering. ii) The onset time, t_{onset} (Ma), to initiate the accretion of a planetesimal from the time of the formation of the CAIs with the canonical value of $(^{26}Al/^{27}Al)_{initial} = 5 \times 10^{-5}$. The case corresponding to $t_{onset} = -0.35$ indicates onset of accretion at the time of formation of CAI with supracanonical value. iii) The accretion duration, $t_{duration}$ (Ma), of the planetesimal. iv) An initial value of 0 (represented as 0[0]), 5×10^{-7} (represented as 5[−7]), 1×10^{-6} (represented as 1[−6]) and 2×10^{-6} (represented as 2[−6]) for the $^{60}Fe/^{56}Fe$ ratio at the time of formation of the CAIs with the canonical value of $(^{26}Al/^{27}Al)_{initial}$. v) The fifth position marks the basic difference regarding the choice of the differentiation scenario. "CI" indicates the CI composition of the planetesimals [Al: 0.84% and Fe: 18.67%]. "2%" corresponds to the segregation of $(Fe\text{-}Ni)_{metal}$ ~2% of the bulk chondrite along with FeS to form an (FeS + Fe[2%]) core. The entire Fe_{metal} and Ni_{metal} contents of the bulk chondrites, i.e., ~16% and ~1.7%, respectively, were segregated along with FeS to form an (FeS + Fe[16%]) core in the remaining simulations. "30" indicates the extrusion of the basaltic melt subsequent to 30% silicate melting. In the remaining set of simulations, the extrusion of basaltic melt was initiated subsequent to 20% silicate melting. "3" or "4" indicate decay energy of 3 and 4 MeV, respectively, for ^{26}Al. We choose a value of 3.16 MeV in the remaining simulations.

[b]Time (Ma) taken for the Fe-FeS core to grow to a specific size. Five different arbitrary choices of the core sizes have been considered. With respect to the final radius of the completely sintered planetesimal, these core sizes are expressed in percentage. In order these are 0+% (initiation of core formation), 10%, 20%, 30%, and 40%. All time spans mentioned in the table are measured with respect to the formation of the CAIs with the canonical value of $(^{26}Al/^{27}Al)_{initial} = 5 \times 10^{-5}$.

[c]Time taken to initiate the basaltic melt extrusion with respect to the formation of the CAIs with the canonical value of $(^{26}Al/^{27}Al)_{initial}$ in the case of the A simulations. However, in the case of the B simulations, this represents the initiation of silicate melting.

planetesimals lost most of their initial FeS melt by volcanism and finally produced sulfur-depleted iron cores. We have not included any possible loss of Fe-FeS melt in our simulations. The melt descent toward the center of the planetesimal to form an iron sulfide core that grows in size according to the thermal evolution of the planetesimal. However, we can infer the possible influence of the FeS loss on the basis of our results.

The latent heats of melting of 2.7×10^5 J kg^{-1} and 4.0×10^5 J kg^{-1} (Table 1) were incorporated into the specific heat during the solidus-liquidus temperature range of Fe-FeS and silicate, respectively, according to the criteria chosen by Merk et al. (2002). A linear relationship was assumed between the generated melt fraction and the temperature within the solidus-liquidus temperature range. The specific heat of ~2000 J kg^{-1} K^{-1} was assumed for the silicate and the Fe-FeS melts (Ghosh and McSween 1998). The specific heat of a particular spatial grid interval was estimated by taking the weighted average of the specific heat of the melt and the solid mass fractions. The Fe-FeS melt generated at a specific spatial grid interval was numerically moved toward the center at a chosen rate of one spatial grid step per temporal grid interval for numerical simplification. The acquired velocity of the descent would be 300 m yr^{-1} in the case of a simulation with a spatial and a temporal grid interval of 300 m and 1 yr, respectively. The descent velocity of 30 m yr^{-1} can be achieved by simply increasing the temporal grid size to 10 yr. Within the precision of the various differentiation time scales quoted in this work (Table 2), we could not find any significant difference in the growth rate of the Fe-FeS core among the simulations with the two distinct descent rates. The densities of the Fe-FeS melt and the bulk chondrite were assumed to be 7800 kg m^{-3} and 3560 kg m^{-3}. The Fe-FeS melt moves toward the center of the planetesimal and replaces silicate that consequently moves upward. This results in the growth of an Fe-FeS core and the formation of a silicate mantle. The differentiation results in the redistribution of ^{26}Al and ^{60}Fe in the mantle and the core, respectively. The silicate matrix in all simulations retained ~8.8% Fe as FeO along with a proportionate amount of ^{60}Fe. Mass balance calculations were carried out at each temporal grid interval to ensure numerical accuracy. The simulations were performed in double precision. The results were analyzed thoroughly to identify any numerical instability. In addition, we systematically studied the numerical range acquired by the numerous parameters, e.g., the specific heat, thermal diffusivity, the (un)melted mass fractions of Fe-FeS and silicate, etc., during the simulations for any inconsistency and instability. In order to thermally imitate the influence of convection in the molten Fe-FeS core, we assumed a hypothetically high thermal diffusivity of 5×10^{-4} m^2 s^{-1} in the set of A simulations. However, we could not incorporate convection in the mantle subsequent to 50% melting of silicate or the emergence of magma ocean (Hevey and Sanders 2006). The inclusion of convection in the mantle will result in an isotropic distribution of heat and an early cooling of planetesimal. In the present work, we avoid discussions on the thermal evolution of the planetesimals subsequent to the emergence of magma ocean.

A basaltic melt was generated subsequent to silicate melting and was moved toward the surface of the planetesimal. In most of the simulations subsequent to the initial, 20% melting of the silicate within a specific spatial grid interval, the entire ^{26}Al content was removed from the silicate matrix. The ascent of the ^{26}Al-rich basaltic melt was parametrically modeled in a discrete manner. The initial 20% silicate melt generated within a specific spatial grid interval was accumulated over time, and finally moved upward in a quantum. The ascent of the melt quantum was executed by moving the quantum at the rate of one spatial grid step per temporal grid interval (the melt percolation velocity). Here, we present results for a specific melt percolation velocity of 300 m yr^{-1} for numerical simplifications. Each of the spatial grid intervals involved in the silicate melting contributed a quantum of basaltic melt. These ^{26}Al-rich silicate melt quanta were gradually moved to the surface of the planetesimals toward the outermost spatial grid interval. In some of the simulations, the extrusion of the basaltic melt was initiated subsequent to 30% silicate melting. It is also possible to model the extrusion of basaltic melt in small discrete quanta carrying 5% silicate melt fractions individually. During their upward ascent through the planetesimal, the heating due to the various ^{26}Al-rich basaltic quanta was considered in the simulations. However, we have not considered the exchange of heat between the ascending quanta and the planetesimal. The possibility of the recrystallization of the basaltic melt while passing through the outer comparatively cooler regions of the planetesimal has not been explored in the present work due to the associated numerical complexities. However, we have considered the complete sintering of the outer insulating regolith layer on account of the gradual extrusion of the basaltic melt to the surface. The associated modification results in complete sintering of the entire planetesimal till the surface spatial grid interval, thereby leading to a rapid cooling of the planetesimals. It should be mentioned that the possibility of the extrusion of the basaltic melt all the way to the surface of the planetesimal and the complete sintering of the regolith is debatable. However, we present results here assuming a complete sintering of the entire planetesimal subsequent to the extrusion of the basaltic melt to the surface. This corresponds to one specific scenario among the multitude of possibilities resulting from the generation of basaltic melt and its extrusion. The assumption regarding the complete sintering of regolith will not only drastically influence the cooling rates of the differentiated planetesimals, the differentiation of small planetesimals (e.g., ≤20 km sized planetesimals) will be terminated earlier.

B Simulations

In these set of simulations, the segregation of the $(Fe\text{-}Ni)_{metal}$-FeS melt to form a Fe-FeS core was initiated subsequent to 40% silicate melting at temperature ≥1630 K (Taylor 1992; Taylor et al. 1993). The $(Fe\text{-}Ni)_{metal}$-FeS melt was generated prior to silicate melting and was retained at its location until 40% silicate melting. We did not perform the crust-mantle differentiation in these simulations. The ^{26}Al-rich silicate melt was retained at the melt region. In the set of B simulations, we have not incorporated the hypothetically high thermal diffusivity of Fe-FeS core to thermally imitate convection, unlike in the A simulations. The planetesimals may finally also acquire a convective mantle subsequent to 50% silicate melting (Hevey and Sanders 2006).

RESULTS

The results obtained from a representative set of simulations are presented in Table 2 along with the simulation details. The time required to initiate the melting of ($[Fe\text{-}Ni]_{metal}$-FeS) in an intermediate-sized planetesimal with a final radius of 50 km undergoing accretion growth is graphically presented in Fig. 1a for three accretion time durations, i.e., 0.001 Ma, 0.1 Ma, and 1 Ma. The results can be generalized for planetesimals with final radii ranging from 20–270 km with the aid of a representative set of simulations for planetesimals sized 20 and 270 km (Fig. 1a). For A simulations, the Fig. 1a indicates the time of the initiation of the formation of the ($[Fe\text{-}Ni]_{metal}$-FeS) core, whereas for B simulations, it merely represents the time of the initiation of the Fe-FeS melt. The initiation of the formation of the ($[Fe\text{-}Ni]_{metal}$-FeS) core for B simulations will occur subsequent to 0.4 fraction melting of silicate. This is presented in Fig. 1b for the three accretion durations, i.e., 0.001 Ma, 0.1 Ma, and 1 Ma. It should be mentioned that there is an alternate and a simple way of deducing the various temporal constraints discussed in Figs. 1a and 1b by considering the exponential decay through time of the remaining radioactive energy per gram of material and the energy needed to cause melting (e.g., Fig. 2 of Sanders and Taylor 2005). We specifically preferred the rigorous numerical method to generate Figs. 1a and 1b in order to generalize the results of a representative set of simulations discussed in Table 2 and Fig. 2. In addition, these figures can be used to verify the accuracy of our thermal models.

The temporal growth of the ($[Fe\text{-}Ni]_{metal}$-FeS) core along with the thermal profiles of the planetesimals with final radii of 20, 50, 100, and 270 km and the initiation of the basaltic melt are presented in Fig. 2 for a selective set of simulations tabulated in Table 2. Numerous simulations with varied parameters (see footnote of Table 2 for parametric details) have been tried to understand the differentiation processes. The various simulation parameters broadly include:

1. The accretion duration in the range of 0.001–1 Ma for the planetesimals of final radii 20, 50, 100, and 270 km. These are the planetesimal sizes subsequent to sintering.
2. The $(^{60}Fe/^{56}Fe)_{initial}$ ratio prevailing at the time of condensation of the CAIs with the canonical and the

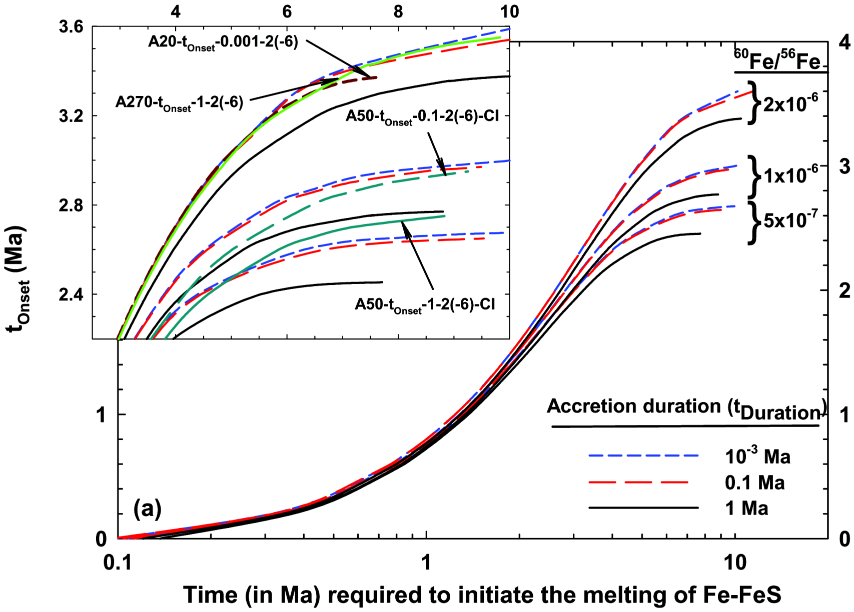

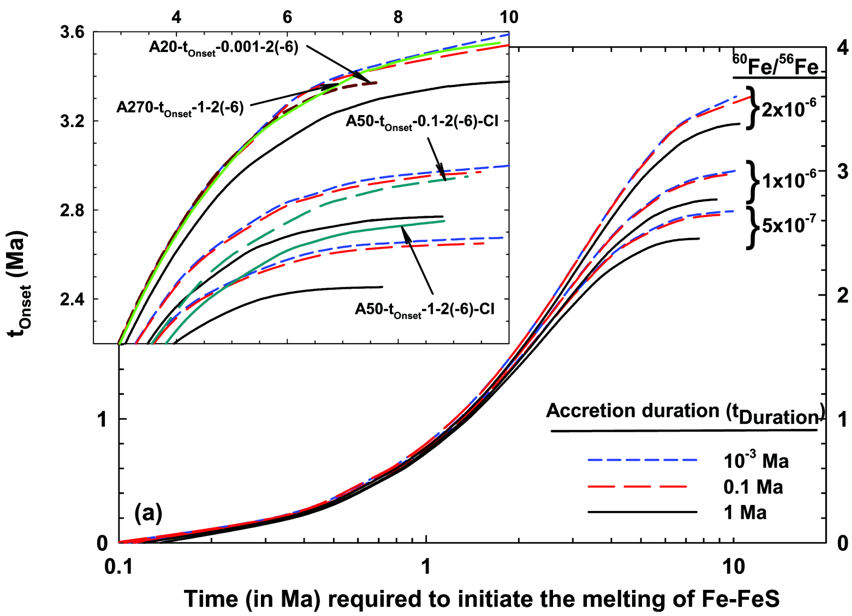

Fig. 1. a) Time required to initiate melting of [$(Fe\text{-}Ni)_{metal}$-FeS] subsequent to the formation of CAIs with the canonical value of 5×10^{-5} for $(^{26}Al/^{27}Al)_{initial}$ at the center of a planetesimal of final radius 50 km for a set of initial $(^{60}Fe/^{56}Fe)_{initial}$ ratios and different accretion durations. The time also indicates the initiation of the core-mantle differentiation in the set of A simulations. b) Time required for 40% melting of silicate subsequent to the formation of the CAIs. The time also indicates the initiation of the core-mantle differentiation in the set of B simulations. The inset in the two figures show the magnified view of a region of the graphs along with the set of four additional simulation runs with the planetesimal radii of 20, 50, and 270 km and distinct chemical composition of the planetesimals (see footnote of Table 2 for details).

supracanonical values of $^{26}Al/^{27}Al$. We have explored a range of $(0–2) \times 10^{-6}$ for the $(^{60}Fe/^{56}Fe)_{initial}$ ratio.

3. The onset time (t_{onset}) of the accretion of the planetesimals subsequent to the condensation of the CAIs with the canonical value of $^{26}Al/^{27}Al$. The simulations (Figs. 1a and 1b) were performed for t_{onset} in the range of −0.35–3.6 Ma. The former time interval corresponds to the onset of the planetesimal accretion at the time of the condensation of the CAI with the supracanonical value of $^{26}Al/^{27}Al$ (Young et al. 2005).
4. The varied proportions of $(Fe + Ni)_{metal}$ segregation during the segregation of FeS in the A simulations.
5. The two distinct criteria chosen for the basaltic melt extrusion subsequent to 20% or 30% silicate melting in the case of set of the A simulations.

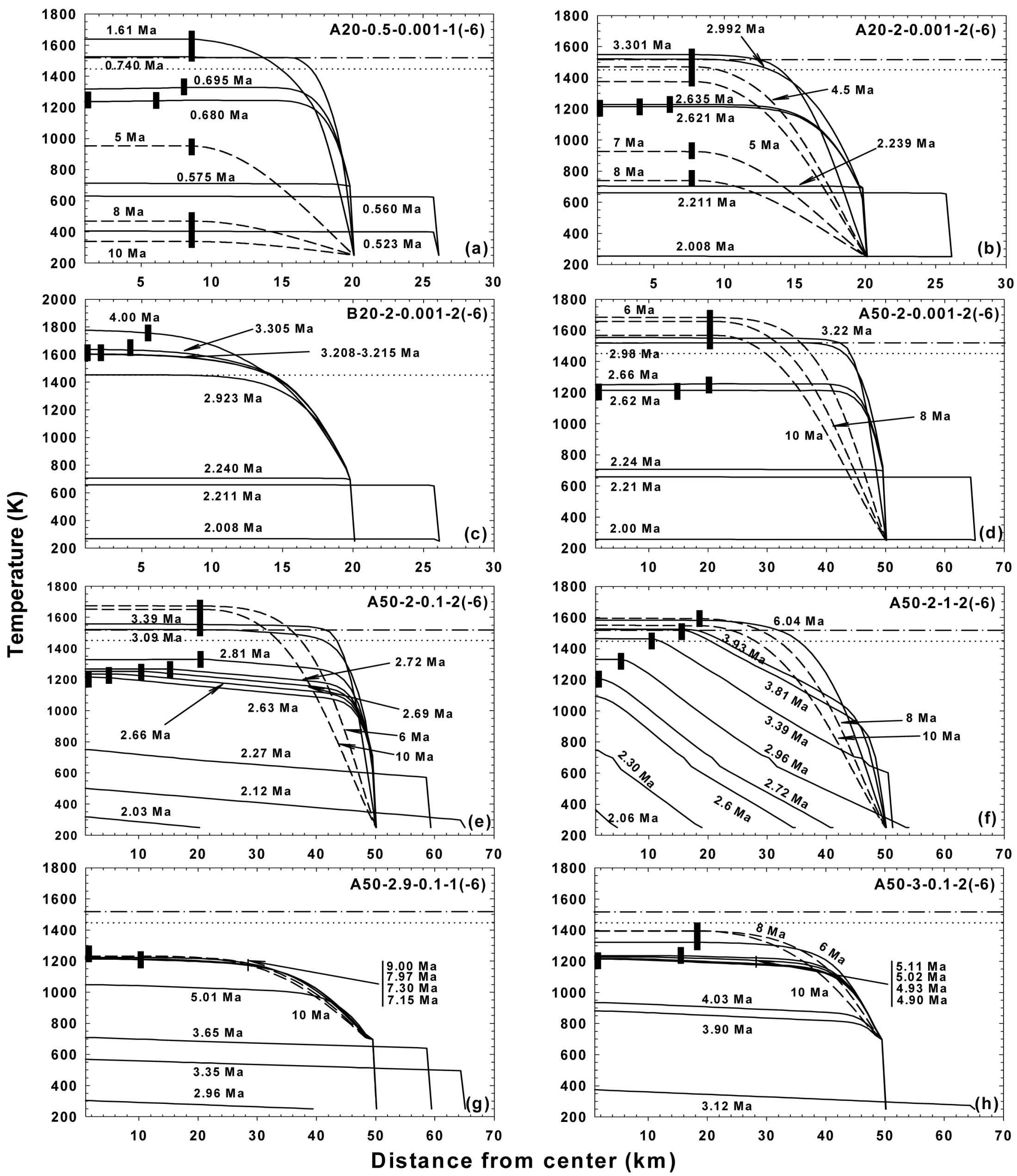

Fig. 2. Thermal profiles of the planetesimals at different epochs during the accretion and differentiation. All time spans are marked with respect to the initiation of the formation of CAIs. The thick vertical bars represent the core size at a given time for a specific thermal profile(s). The horizontal dot-dashed line indicates 20% silicate melting for the extrusion of the basaltic melt. The horizontal dotted line represents the solidus temperature of silicate (1450 K). The thermal profiles subsequent to the cooling of the planetesimals are represented by dashed curves for an easier view.

DISCUSSION

Detailed thermal models for the differentiation of planetesimals undergoing accretion growth with ^{26}Al and ^{60}Fe as the heat sources have been developed. The aim is to understand the dependence of the core-mantle and the mantle-crust differentiation on the onset time of the planetesimal accretion subsequent to the condensation of CAIs, the duration of the planetesimal accretion, the abundance of the radionuclides, and the distinct planetary differentiation criteria. Since there are several parameters involved in deducing the thermal history of the planetesimals, we intend to present here a much broader representation of the temporal scales involved in the differentiation of planetesimals rather than imposing precise temporal constraints.

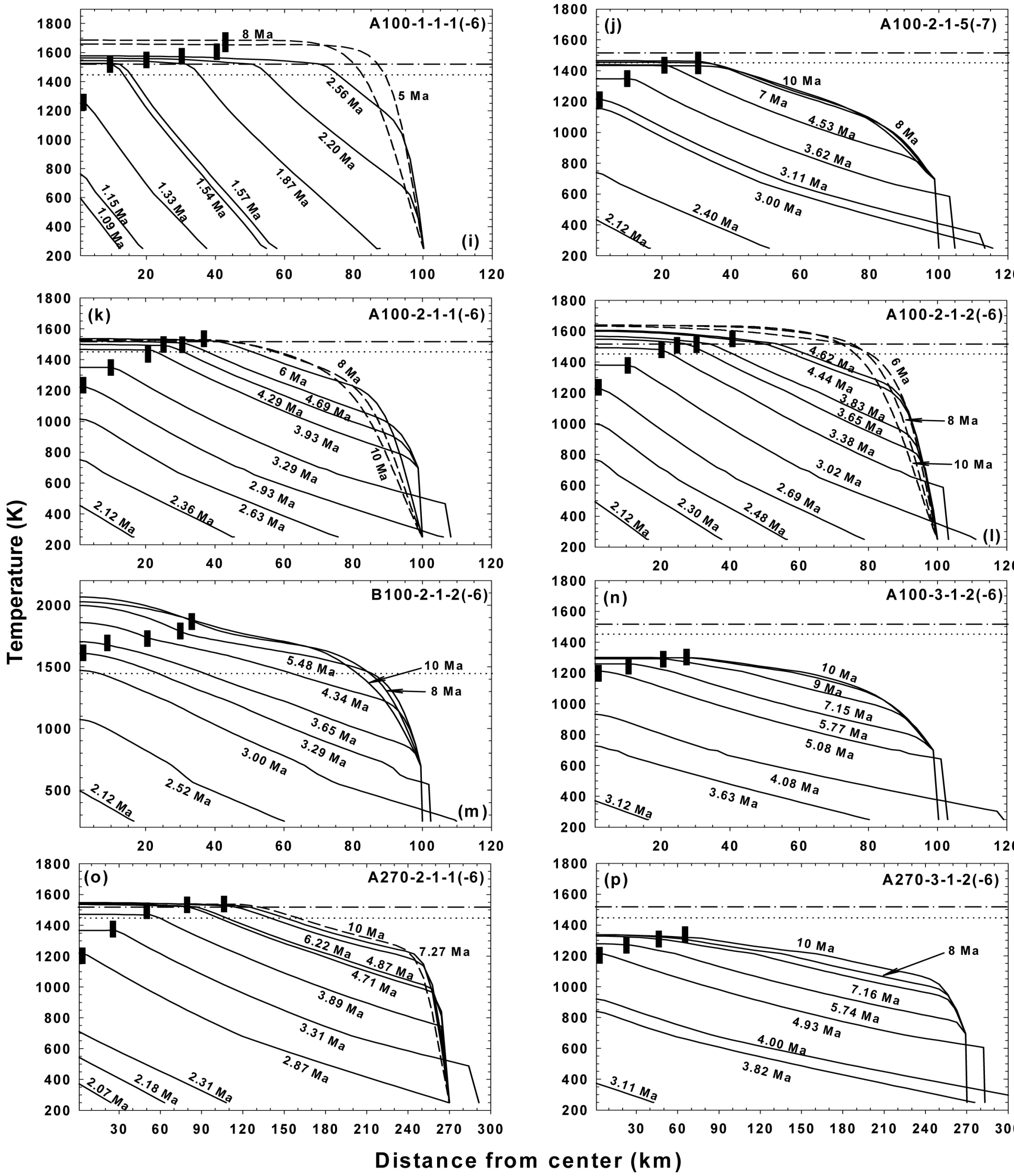

Fig. 2. *Continued.* Thermal profiles of the planetesimals at different epochs during the accretion and differentiation. All time spans are marked with respect to the initiation of the formation of CAIs. The thick vertical bars represent the core size at a given time for a specific thermal profile(s). The horizontal dot-dashed line indicates 20% silicate melting for the extrusion of the basaltic melt. The horizontal dotted line represents the solidus temperature of silicate (1450 K). The thermal profiles subsequent to the cooling of the planetesimals are represented by dashed curves for an easier view.

The Core-Mantle Differentiation

The Initiation of the Fe-FeS Core Formation

In order to study the dependence of the onset time of the melting of Fe-FeS on the various simulation parameters, we considered a representative case of an intermediate-sized planetesimal with a radius of 50 km. The results were further generalized for varied sizes ranging from 20–270 km using 20 km and 270 km planetesimals (Fig. 1a). Furthermore, we also studied the influence of the elemental abundances of Al and Fe in the planetesimals. The CI composition (Dodd 1981) was chosen in a representative set of simulations (Figs. 1a and 1b). Among the several simulation parameters, the time of the initiation of the ($[Fe\text{-}Ni]_{metal}$-FeS) melting depends strongly upon the onset time (t_{onset}) of the accretion of a planetesimal (Fig. 1a). This time increases steadily from ~0.1 Ma and extends to 7–10 Ma with the increase in t_{onset} for a 50 km sized (radius) planetesimal (Fig. 1a). Beyond a certain range of t_{onset}, it is not possible to melt Fe-FeS to cause differentiation. This is marked by a decline in the slope of the various curves corresponding to distinct set of simulation parameters (Fig. 1a) beyond a certain range of t_{onset}. In general, the initiation of the melting of Fe-FeS due to the decay of ^{26}Al and ^{60}Fe would be broadly confined to <10 Ma of the early solar system (Fig. 1a). This upper temporal constraint can alter from 7–10 Ma depending on the various simulation parameters, specifically, the chosen (^{60}Fe/^{56}Fe)$_{initial}$ ratio and the assumed Al and Fe elemental abundances. Since we have carried out most of the simulations for the Fe-rich H chondrites, the various inferences drawn regarding the temporal extent of differentiation of planetesimals in the early solar system exclusively due to the decay energy of ^{26}Al and ^{60}Fe would provide an upper limit.

A faster accreting ($t_{duration} \leq 0.1$ Ma) planetesimal or a planetesimal accreted with a high (^{60}Fe/^{56}Fe)$_{initial}$ ratio attains the Fe-FeS melting temperature rapidly (Fig. 1a), hence leading to an early initiation of the core-mantle differentiation in the A simulations. The elemental abundances of Al and Fe in the planetesimal significantly influence the onset time of Fe-FeS melting and the core-mantle differentiation (Fig. 1a). Depending on the accretion scenario and the (^{60}Fe/^{56}Fe)$_{initial}$ ratio, the initiation of the accretion of a planetesimal of radius 50 km and CI elemental abundance should occur within the initial ~3 Ma in order to result in Fe-FeS melting. The accretion of a planetesimal of H-chondrite composition, with comparatively high Al and Fe, should initiate within the initial ~3.6 Ma of the early solar system (Fig. 1a). Compared to the planetesimals with CI composition, the planetesimals with H-chondrite composition will experience quite early initiation of the melting of Fe-FeS and an early core-mantle differentiation. In general, the initiation of the core-mantle differentiation of the bodies with H-chondrite and CI-chondrite compositions could commence during the initial ~10 Ma and ~8 Ma, respectively (Fig. 1a). However, this does not imply that the subsequent melting and differentiation of the planetesimal would continue beyond this upper temporal scale. The further melting and the differentiation would cease in the case the various curves in the Fig. 1 approach a zero slope.

The planetesimal size also influences the Fe-FeS melting and core-mantle differentiation. Compared to the case of an instantaneous accretion of an intermediate-sized planetesimal with a radius of 50 km where the initiation of the Fe-FeS melting could occur over the initial ~10 Ma with $t_{onset} \leq 3.6$ Ma, the initiation of the Fe-FeS melting in a planetesimal 20 km in size would be confined to the initial ~7 Ma with $t_{onset} \leq 3.3$ Ma. A planetesimal 270 km in size accreted over a time scale of 1 Ma will follow a temporal trend in the initiation of the Fe-FeS melting similar to a planetesimal 50 km in size accreted over a time scale of 0.1 Ma (Fig. 1a).

In order to initiate core-mantle differentiation in the B simulations, the planetesimal accretion should initiate within the initial ~2.8 Ma of the early solar system (Fig. 1b). These set of simulations require 0.4 fraction silicate melting to initiate core-mantle differentiation, hence requiring a greater extent of planetesimal melting compared to the A simulations. Depending on the accretion scenario, the size of the planetesimal, the planetesimal composition, and the (^{60}Fe/^{56}Fe)$_{initial}$ ratio, the initiation of the core-mantle differentiation in most of the B simulations can broadly commence during the initial ~8 Ma in the early solar system (Fig. 1b). In general, the core-mantle differentiation in the A simulations can be initiated ~0.1–6 Ma earlier compared to the B simulations run with identical simulation parameters (Figs. 1a and 1b). The onset time of the accretion of the planetesimals will critically decide the temporal lag between the initiations of the core-mantle differentiation in the two distinct differentiation scenarios.

Growth of the Fe-FeS Core

Subsequent to the initiation of the formation of the Fe-FeS core, the further growth of the core again depends primarily on the choice of the differentiation criteria among the various alternatives tried in the present work (Table 2; Fig. 2). The growth will also depend on the varied proportions of (Fe + Ni)$_{metal}$ segregation during the segregation of FeS in the case of the A simulations (Table 2). For a specifically chosen differentiation criteria, the growth of the core is primarily governed by the accretion rate of the planetesimal. The growth is rapid in the case of fast accretion ($t_{duration} \sim 0.001$ Ma), whereas the growth occurs over several million years in the case of slow accretion ($t_{duration} \geq 1$ Ma) (Table 2; Fig. 2). The onset time of the planetesimal accretion (t_{onset}), the final size of the planetesimal, the elemental composition of the planetesimal, and the (^{60}Fe/^{56}Fe)$_{initial}$ ratio will also influence the growth of the core (Table 2).

Growth of the Fe-FeS Core in Rapidly Accreted Small Planetesimals

As the small planetesimals are likely to have accreted rapidly in the early solar system, we chose planetesimals 20 and 50 km in size with fast accretion growth ($t_{duration} \sim 0.001$ Ma) as representative cases to understand the differentiation of small bodies. Except for the outer ~5 km, these rapidly accreting planetesimals resulted in almost isothermal interiors at different epochs prior to the melting and segregation of Fe-FeS (Figs. 2a–d). The temperature differences between the center and the outer regions of the planetesimals are a few K in the initial stages of the simulations, hence the accretion over 0.001 Ma can be treated as almost instantaneous. In majority of the A simulations with the planetesimal having a final radius of

20 km, $t_{duration} \sim 0.001$ Ma, and $t_{onset} < 3$ Ma, the growth of the inner 4–6 km Fe-FeS core is almost instantaneous within the precision quoted in Table 2 and Figs. 2a and 2b. Identically, in the case of a planetesimal 50 km in size, $t_{duration}$ ~0.001 Ma and t_{onset} <3 Ma, the inner core 15–20 km in size grows almost instantaneously (Table 2; Fig. 2d). The remaining growth of the core in the planetesimal with a final radius of 20 km occurs in ≤0.1 Ma. In simulation A20-3-0.001-2(-6), the growth of the 4 km core occurs over 0.2 Ma. This is essentially due to the relatively late onset of the planetesimal accretion (t_{onset} = 3 Ma) compared to the other simulations. The growth of the core is truncated at ~4 km with the radioactive heating not sufficient to further cause differentiation. Identically, in the A simulations with the planetesimal with a final radius of 20 km and t_{onset} = 2 Ma, the core growth is truncated at ~6 km. The higher value of 2×10^{-6} for the $(^{60}Fe/^{56}Fe)_{initial}$ ratio in case of A20-2-0.001-2(-6) compared to the value of 5×10^{-7} and 1×10^{-6} in A20-2-0.001-5(-7) and A20-2-0.001-1(-6), respectively, provides an early and rapid differentiation. An Fe-FeS core ~7.5 km (Fig. 2b) is formed in A20-2-0.001-2(-6). Further growth of the core is truncated due to thermal losses from the surface on account of basaltic melt extrusion and complete sintering of the planetesimal at ~2.992 Ma.

Compared to the almost instantaneous growth of the inner 6 km Fe-FeS core in A20-2-0.001-2(-6), the simulation B20-2-0.001-2(-6), with identical simulation parameters, results in comparatively prolonged growth of the 4 km core over a time span of ~0.1 Ma. The core-mantle segregation in the latter case is triggered subsequent to 0.4 fraction melting of the silicate. Due to the small final radius of 20 km, the planetesimal loses heat rapidly before acquiring temperature for 0.4 fraction melting of the silicate. This results in a slow growth of a small core in simulation B20-2-0.001-2(-6). Identically, simulation B20-1-0.001-2(-6) results in a prolonged formation of the core 8 km in size compared to simulation A20-1-0.001-2(-6). In summary, for a rapid and a planetary scale core-mantle differentiation, the accretion of the planetesimal should commence early in the solar system over time scales comparable to that inferred for the formation of CAIs and chondrules (Table 2; Figs. 1a and 1b) This is consistent with the ^{182}Hf-^{182}W isotopic systematics of the majority of the iron meteorites (Kleine et al. 2005a, 2005b; Bizzarro et al. 2004, 2005, 2006a, 2006b; Markowski et al. 2006; Scherstén et al. 2006; Qin et al. 2006; Bottke et al. 2006). In the present work, the simulations with t_{onset} = 0 and −0.35 Ma correspond to the instantaneous accretion growth of a planetesimal 20 km in size at the time of the formation of the CAIs with the canonical and the supracanonical values of $^{26}Al/^{27}Al$, respectively (Table 2). In these scenarios, the 6 km sized core is formed within a short interval of ~0.1 Ma, with the extrusion of the basaltic melt within the initial ~0.15 Ma from the onset of the planetesimal accretion. In some of these scenarios the rapid differentiation of planetesimals occurs in the absence of ^{60}Fe as indicated by Bizzarro et al. (2006b).

Growth of the Fe-FeS Core in Slowly Accreted Planetesimals

Major differences in the growth rate of core were not observed as the accretion duration of the planetesimals ($t_{duration}$) was increased from 0.001 to 0.01 Ma. This is evident from simulations A50-2-0.01-2(-6) and A50-2-0.001-2(-6) (Table 2). These simulations resulted in almost instantaneous growth of the inner 15 km core with slight differences in the further growth from 15–20 km. The extrusion of the basaltic melt in these two models occurred within a time gap of 0.01 Ma. These scenarios also resulted in almost isothermal interiors (e.g., Fig. 2d) at different epochs prior to the melting and segregation of Fe-FeS.

The differences in the growth rate of core become significant as $t_{duration}$ is increased to 0.1 Ma. Simulations A20-2-0.1-1(-6), A20-2-0.1-2(-6), A50-2-0.1-2(-6), and A100-2-0.1-2(-6) result in prolonged core formation compared to simulations A20-2-0.001-1(-6), A20-2-0.001-2(-6), A50-2-0.001-2(-6), and A100-2-0.001-2(-6), respectively. The growth of the 6 km sized core in A20-2-0.1-2(-6) occurs over 0.1 Ma, whereas the 40 km sized core in A100-2-0.1-2(-6) takes 0.14 Ma to grow subsequent to the initiation of the core formation. Simulations A20-2-0.1-1(-6), A20-2-0.1-2(-6), A50-2-0.1-1(-6), A50-2-0.1-2(-6), A50-2.9-0.1-1(-6), A50-3-0.1-2(-6), and A100-2-0.1-2(-6) resulted in larger negative thermal slopes at different epochs prior to the melting and segregation of Fe-FeS (see e.g., Figs. 2e, 2g, and 2h) compared to the simulations with $t_{duration}$ ≤ 0.01, which yielded almost isothermal interiors. For example, the slopes of the thermal profiles subsequent to the completion of the planetesimal accretion in simulation A50-2-0.1-2(-6) are ~3 K km^{-1}. The basaltic melt extrusion in the case of simulations with $t_{duration}$ = 0.1 Ma occurs ~0.1 Ma after the basaltic melt extrusion in the case of simulations with $t_{duration}$ ≤ 0.01 Ma (Table 2).

In general, the growth rate of the Fe-FeS core is retarded considerably for $t_{duration}$ > 0.1 Ma. Numerous simulations have been attempted with the final planetesimal radii of 50, 100, and 270 km to study the growth of Fe-FeS core for $t_{duration}$ = 1 Ma and a varied range of other parameters (Table 2). These simulations, e.g., [A and B]50-2-1-2(-6), A100-1-1-1(-6), A100-[0.5,1,3]-1-2(-6), [A and B]100-2-1-2(-6), A270-[0.5,2]-1-1(-6), and A270-[0.5,1,2,3]-1-2(-6) indicate a prolonged growth of core over a time span of 1–5 Ma after the initiation of the core formation (Table 2). For example, the initiation of the core formation in A100-1-1-1(-6) commences at 1.33 Ma and the 40 km sized core is formed by 2.56 Ma (Fig. 2i), whereas the core formation is initiated at 5.08 Ma in A100-3-1-2(-6) and the ~27 km sized core is gradually formed by ~9 Ma (Fig. 2n). Identically, in A270-3-1-2(-6) (Fig. 2p), the core formation could have continued for ≤10 Ma of the early solar system. The last two scenarios with a $(^{60}Fe/^{56}Fe)_{initial}$ ratio of 2×10^{-6} indicate a temporal scale of ≤10 Ma for the core-mantle differentiation of planetesimals of H-chondrite composition in the early solar system with ^{26}Al and ^{60}Fe as the exclusive heat sources. However, in simulations with the ($^{60}Fe/^{56}Fe$)$_{initial}$ ratio of 1 × 10^{-6}, e.g., simulations A100-2-1-1(-6) and A270-2-1-1(-6) (Figs. 2k and 2o), the melting and core-mantle differentiation could have occurred over the initial ~6–7 Ma (Table 2) in the early solar system. Along with simulation A50-2.9-0.1-1(-6) with $t_{duration}$ = 0.1 Ma, we generally do not anticipate significant melting and differentiation to extend beyond ~7–8 Ma for the simulations with ($^{60}Fe/^{56}Fe$)$_{initial}$ ratio of 1× 10^{-6} (Fig. 1a). A lower ($^{60}Fe/^{56}Fe$)$_{initial}$ ratio and/or a lower iron content of the planetesimal would further reduce the temporal extent of significant melting and core-mantle differentiation exclusively due to the radioactive heating. This in turn could impose a stringent constraint on the validity of the radioactive decay energy as the exclusive heat source in context with the observed protracted core-mantle differentiation in the Eagle Station pallasite parent body (Dauphas et al. 2005). The parent body of the pallasite, with a CV composition, would probably require an additional heat source for the planetary differentiation.

The simulations with $t_{duration}$ = 1 Ma resulted in thermal profiles with larger negative slopes at different epochs prior to the melting and segregation of Fe-FeS (Fig. 2) compared to the simulations with $t_{duration}$ ≤ 0.1 Ma. For example, subsequent to the initiation of the planetesimal accretion and prior to the planetesimal sintering in simulations A50-2-1-2(-6), A100-1-1-1(-6), and A270-3-1-2(-6) (Figs. 2f, 2i, and 2p), we inferred slopes of ~−25, −29, and −2 K km^{-1}, respectively. The lower values in the case of A50-2-1-2(-6) and A100-1-1-1(-6) compared to A270-3-1-2(-6) are due to the slower accretion rates (50–100 km Ma^{-1}) of the 50 and the 100 km sized planetesimals compared to the accretion rate of 270 km Ma^{-1} in A270-3-1-2(-6). The additional cause of the major difference could be due to the different onset times of the planetesimals accretion. The abundances of ^{26}Al and ^{60}Fe have declined considerably by the time the 270 km sized planetesimal have started forming.

We have performed several simulations with varied values of the ($^{60}Fe/^{56}Fe$)$_{initial}$ to study its dependence on the simulations with slowly accreted planetesimals. As mentioned earlier, significant differences in the growth rate of Fe-FeS core were found due to the differences in the assumed ($^{60}Fe/^{56}Fe$)$_{initial}$. Simulation A100-2-1-2(-6) resulted in a faster growth of the core compared to A100-2-1-1(-6) and A100-2-1-5(-7). Identical results were obtained for the planetesimal 20 km in size. The ($^{60}Fe/^{56}Fe$)$_{initial}$ ratio (Mostefaoui et al. 2004, 2005; Tachibana and Huss 2003) prevailing in the early solar system is extremely important in deciphering the thermal evolution and the differentiation of planetesimals, specifically in the Fe-rich H chondrites studied in this work. Even though we have tried to understand its dependence on the planetary differentiation process (Figs. 1a and 1b; Table 2), most of the simulations presented in Table 2 and Fig. 2 were run with a ($^{60}Fe/^{56}Fe$)$_{initial}$ ratio of 10^{-6} and 2 × 10^{-6}. The former ratio is based on the $^{60}Fe/^{56}Fe$ ratio inferred from the troilite grains from Semarkona meteorite (Mostefaoui et al. 2005), whereas the latter represents the extrapolated ($^{60}Fe/^{56}Fe$)$_{initial}$ of ~1.8 × 10^{-6} (treated here as 2 × 10^{-6}) at the time of the formation of CAIs if we assume that the troilite grains from Semarkona meteorite have the same age as its chondrules (Mostefaoui et al. 2005). In addition, a couple of simulations were carried out with an ($^{60}Fe/^{56}Fe$)$_{initial}$ ratio of 5 × 10^{-7} (Tachibana and Huss 2003). It should be mentioned that at present there is a large uncertainty in deducing the ($^{60}Fe/^{56}Fe$)$_{initial}$ in the early solar system. There is even speculation that ^{60}Fe was injected late in the solar nebula (Bizzarro et al. 2006b). We have also investigated this possibility.

The Extrusion of the Basaltic Melt and the Formation of Crust

The initiation and the subsequent extent of silicate melting in a planetesimal depend primarily on the onset time of the accretion (t_{onset}) of the planetesimal. The accretion duration ($t_{duration}$), the elemental composition of planetesimal, the ($^{60}Fe/^{56}Fe$)$_{initial}$ ratio, and the size of the planetesimal also influence silicate melting. In the case of t_{onset} ≥ 3 Ma, the silicate melting does not occur (Table 2). The dependence of the ($^{60}Fe/^{56}Fe$)$_{initial}$ ratio in the range (0–2) × 10^{-6} on silicate melting of the planetesimals of final radii 20 and 100 km with the accretion duration of 0.001 Ma and 1 Ma is presented in Table 2. The silicate melting and the basaltic melt extrusion in the case of A20-2-0.001-5(-7) takes place due to the rapid accretion of the planetesimal. In contrast to this simulation, the basaltic melt extrusion to the surface was not observed in A100-2-1-5(-7) due to the slow accretion growth of the 100 km sized planetesimal in spite of its larger size.

Based on the representative set of simulations, the initiation of the basaltic melt extrusion to the surface of a planetesimal could have occurred within the initial ~4 Ma of the early solar system (Table 2). Subsequent melting of silicate could have persisted over the initial ~7–8 Ma in the early solar system. This inference can be drawn from simulations A100-2-1-1(-6), A100-2-1-2(-6), and A270-2-1-1(-6), where the silicate melting continued until ~7–8 Ma (Figs. 2k, 2l, and 2o). In general, due to the radioactive heating in the large planetesimals (radii 50 km), the silicate melting, leading to the production of basaltic melt, could have continued at least over the initial ~8 Ma of the early solar system. This is consistent with the ^{26}Al-^{26}Mg and ^{53}Mn-^{53}Cr systematics in eucrites and angrites where the crust-mantle differentiation occurred quite early in the early solar system (Srinivasan et al. 1999; Srinivasan 2002; Nyquist et al. 2001, 2003a, 2003b, 2003c; Baker et al. 2005; Bizzarro et al. 2005; Markowski et al. 2006).

For the small bodies, e.g., the planetesimals 20 km in size (Fig. 2), the silicate melting was essentially confined to the initial ~4 Ma of the early solar system due to the extensive thermal losses. This temporal constraint can be obtained from simulations A20-2-0.001-5(-7) and A20-2-0.001-2(-6), where the silicate melting occurred at ~4.1 and ~3 Ma, respectively. In the latter, the silicate melting persisted for an additional ~0.3 Ma (Fig. 2b). It should be noted that due to the extrusion of the basaltic melt to the surface and the complete sintering of the insulating regolith layer, even the planetesimals with sizes >20 km experienced significant thermal losses. This resulted in an early termination of silicate melting in these planetesimals.

Comparisons Among the Various Differentiation Scenarios

In the present work, the two sets of simulations A and B were performed to explore the two extremely contradictory views regarding the temporal sequence of the core formation with respect to silicate melting and the crust formation (e.g., Ghosh and McSween 1998). In the A simulations, the formation of core commences prior to silicate melting, whereas in the B simulations, core formation occurs subsequent to 0.4 fraction of silicate melting. The reality may lie between these two extremes. The growth of the Fe-FeS core and the thermal evolution of the planetesimals are different for the two extremely distinct criteria chosen for the core-mantle differentiation. The set of A simulations triggers an early core-mantle differentiation and thus an early segregation of ^{60}Fe. The major difference in the two sets of simulations is the manner in which the silicate melting proceeds. The initiation of the silicate melting takes place at the center, and the melting gradually extends toward the outer regions of the planetesimal in the B simulations, e.g., B50-2-1-2(-6), B100-2-0.1-2(-6), and B100-2-1-2(-6) (see, e.g., Fig. 2m).

However, in the A simulations, the silicate melting initiates in a narrow region ≤10 km, right above the core-mantle transition, e.g., A100-1-1-1(-6) (Fig. 2i). This narrow region of silicate melting moves as a front in an outward direction with the growth of the core. The removal of the ^{26}Al-rich basaltic melt from the melt region influences the subsequent thermal evolution and the melting of the silicate. The extrusion of the basaltic melt to the surface causes complete sintering of the surface regolith. The further rise in the temperature of the convective Fe-FeS core and the silicate mantle is controlled by the thermal losses from the sintered surface. This in turn influences the extent of further silicate melting.

It should be noted that in the simulations with t_{onset} < 1 Ma and t_{duration} = 1 Ma, the basaltic melt extrusion to the surface occurs even prior to the complete accretion of the planetesimal. The further accretion of the planetesimal occurs along with simultaneous differentiation and the extrusion of the basaltic melt. It is essential to understand the extent of the basaltic melt extrusion to the surface and the extrusion velocity of the basaltic melt specifically in these scenarios.

The extrusion of the basaltic melt at 30% silicate melting (A100-0.5-1-2[-6]-30) resulted in an earlier growth (~0.03 Ma early) of the 40 km sized core compared to the simulation A100-0.5-1-2(-6), where the extrusion occurred at 20% silicate melting (Table 2). This may be due to the early sintering of the regolith layer in the latter case that resulted in delayed formation of the outer ~10 km core. No significant differences were observed in A20-0.5-0.001-2(-6) and A20-0.5-0.001-2(-6)-30 as the core formation in the two cases occurred prior to basaltic melt extrusion.

In simulations A50-2-1-2(-6)-2% and A100-2-1-2(-6)-2% (Table 2), the growth of the (FeS + Fe[2%]) core initiates prior to silicate melting. Substantial segregation of $(\mathrm{Fe\text{-}Ni})_{\mathrm{metal}}$ can occur in this scenario subsequent to the initiation of silicate melting. However, in the present work, most of the simulations were terminated above the silicate melting due to the increase in the numerical complexities. A realistic model may involve growth of an Fe-S-FeNi core, subsequently followed by $(\mathrm{Fe\text{-}Ni})_{\mathrm{metal}}$ segregation during the silicate melting. Wasson and Huber (2006) have proposed an identical scenario for the formation of IID iron meteorites. This model is beyond the scope of the present work.

As mentioned earlier, the partial loss of Fe-FeS by explosive volcanism has been proposed by Keil and Wilson (1993) to explain the sulfur depletion in several groups of iron meteorites. Even though we have not accounted for the loss in our simulations, the influence of the loss can be quantitatively accessed. It is likely that the Fe-FeS melts generated in models A50-2-1-2(-6)-2% and A100-2-1-2(-6)-2% were at least partially lost by the planetesimals due to early volcanism. The loss would be more prominent in small planetesimals (a few tens of km in size), specifically, if the melting occurred during the initial stages of the growth of the planetesimal. This would result in the partial depletion of Fe-FeS. Subsequent to $(\mathrm{Fe\text{-}Ni})_{\mathrm{metal}}$ segregation during silicate melting, a sulfur-depleted $(\mathrm{Fe\text{-}Ni})_{\mathrm{metal}}$ core would be formed. The size of this core can be deduced by deducting the FeS contents of the Fe-FeS core produced in the B simulations.

Finally, it should be mentioned that an early onset of a planetesimal accretion with t_{onset} < 0.5 Ma could eventually lead to peak temperatures ~2000 K. The production of chondrules by the collisions of these molten planetesimals has been suggested by Sanders (1996) and Sanders and Taylor (2005). The set of B simulations that requires substantial silicate melting prior to the core-mantle differentiation would be relevant to understand this mechanism of chondrule formation.

Apart from understanding the growth of Fe-FeS core, our thermal models could help to constrain the latest time in the early solar system that melting can occur to produce basalt. The chronological records of the majority of the basaltic meteorites indicate ages of 3 Ma or younger, compared to the CAIs with the canonical value of ^{26}Al/^{27}Al. Even though these records are consistent with our simulations results, there is a surprising lack of the older basalts in spite of the predictions of even early mantle-crust differentiation by our thermal models (see e.g., Fig. 1b). However, the early formation of iron cores is consistent with the chronological records of the iron meteorites.

Comparisons Among the Thermal Models Developed by Various Groups

In order to make comparisons of our simulations with the thermal models developed previously by several groups (Ghosh and McSween 1998, 1999; Ghosh et al. 2003; Bizzarro et al. 2005; Hevey and Sanders 2006), we ran several additional simulations (Fig. 3). These simulations were run with most of the parameters identical to the parameters chosen by different groups. We did not invoke thermal convection in the Fe-FeS core in any of these simulations.

Simulation B50-0.75-0.001 (Fig. 3a) for the planetesimal 50 km in size with t_{onset} = 0.75 Ma and $t_{duration}$ = 0.001 Ma yielded thermal profiles almost identical to those obtained recently by Hevey and Sanders (2006). This includes the thermal evolution of the planetesimal subsequent to its consolidation at ~700 K. In spite of the slightly different approach followed for sintering in the two works, the results are identical. The ^{60}Fe contribution to the planetesimal heating was excluded in this simulation. ^{26}Al decay energy of 4 MeV and Al concentration of 0.9% by mass were chosen. The specific heat variation from 650 to 1250 J kg^{-1} K^{-1} over the temperature range of 250–1850 K was considered (Hevey and Sanders 2006). The differences in the thermal profiles beyond 1.42 Ma (Fig. 3a) are essentially due to the distinct criteria chosen for the subsequent evolution of the planetesimal. In the present case, we initiated the core-mantle differentiation subsequent to 40% melting of the silicate, whereas Hevey and Sanders (2006) considered convection in the melted planetesimal without invoking core-mantle differentiation.

It should be noted that in the case of rapid accretion of a planetesimal (e.g., Figs. 2a–d), the consolidation of the planetesimal at 670–700 K occurred throughout the body at almost the same time. This resulted in an almost isothermal profile during the consolidation of the bodies. This is consistent with the results obtained by Hevey and Sanders (2006). However, in simulations with $t_{duration}$ = 1 Ma, a slight discontinuity in the slopes of thermal profiles were observed at the sintering temperatures. This slight discontinuity marks a broad region of ~5 km that is partially sintered and is in the process of consolidation. The region beneath this discontinuity is completely sintered, whereas the region above the discontinuity is fully unconsolidated. It would be essential for future researchers to further investigate the issues related with these discontinuities, the regolith thickness, and the influence of the basaltic melt extrusion on the sintering of regolith.

Using the simulation parameters of Ghosh and McSween (1998), we ran simulation A270-2.85-0.01-2(-8) for a planetesimal 270 km in size (final radius) (Fig. 3c) with t_{onset} = 2.85 Ma, $t_{duration}$ = 0.01 Ma, $(^{60}Fe/^{56}Fe)_{initial}$ ratio of 2×10^{-8}, and an Al abundance of 1.13% by weight. The initial temperature of 292 K was assumed with the surface maintained at the same temperature through out the simulation. The variation of the specific heat with temperature was considered to be identical to those used by Ghosh and McSween (1999). We observed no core-mantle differentiation in this scenario. This is in contrast to the core-mantle-crust differentiation observed by Ghosh and McSween (1998). However, our results are consistent with the analytical solutions of the partial differential equation with a constant specific heat of ~800 J kg^{-1}K^{-1} and a constant surface temperature of 292 K. We obtained a maximum temperature of ~900 K at ~7.9 Ma (Fig. 3c) that is low by a factor of ~1.4 to initiate core-mantle differentiation. In order to obtain results identical to those of Ghosh and McSween (1998), we ran simulation A270-2.85-0.01-2(-8)-LS (here, LS stands for low specific heat) with the specific heat reduced by a factor of 2 compared to the one used in the remaining simulations (Fig. 3d). This simulation resulted in core-mantle differentiation, subsequently followed by silicate melting. It is difficult to exactly find out the cause of the major differences observed among the two works. Ghosh and McSween (1998) used the finite element method with the radiation boundary condition, whereas we have used finite difference method with a constant surface temperature. Even though the former scenario is expected to result in a comparatively hotter planetesimal inner, it is difficult to quantify the differences in the results obtained from the two approaches.

We ran another simulation, A100-3.4-0.01, with the simulation parameters identical to those used by Ghosh and McSween (1999) for a H-chondrite parent body (Fig. 3b). A constant specific heat of ~800 J kg^{-1} was used. We obtain a peak temperature of ~600 K that is again low by a factor of ~1.5 compared to the results obtained by Ghosh and McSween (1999). We anticipate identical differences in the results of simulating thermal metamorphism of 6 Hebe (Ghosh et al. 2003).

Finally, in order to make comparisons of our thermal models with those developed by Bizzarro et al. (2005), we ran several simulations with t_{onset} in the range of 0 to 0.8 Ma. The $t_{duration}$ was considered to be 0.001 Ma. We chose a planetesimal 100 km in size with a constant surface temperature of 200 K, an Al abundance of 0.85% by weight, and decay energy of 3 MeV for ^{26}Al (H. Haack, personal communication). We chose the B simulation criteria for the core-mantle differentiation of a planetesimal 100 km in size. However, the core-mantle differentiation was triggered at 1723 K (Bizzarro et al. 2005). We made an attempt to reproduce the planetesimal melting trend for ^{26}Al of Fig. 2a of

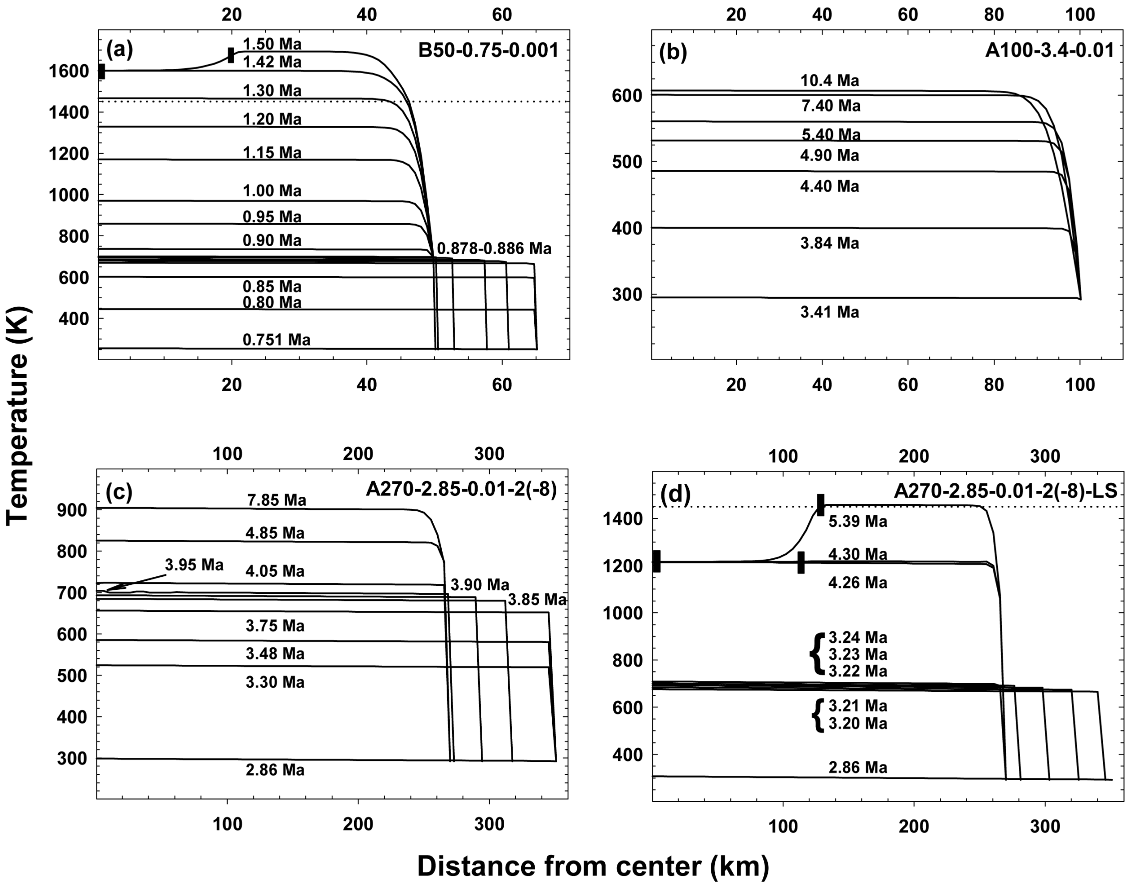

Fig. 3. Same as Fig. 2.

Bizzarro et al. (2005). For the 50% silicate melting, we obtained the times of 0.4, 0.7, 1.13, 1.6, and 2.2 Ma corresponding to t_{onset} of 0.0, 0.2, 0.4, 0.6, and 0.8 Ma, respectively. In general the trend is consistent with that obtained by Bizzarro et al. (2005) until t_{onset} ~0.4 Ma. Subsequent departure in the melting trend for higher values of t_{onset} could be due to differences in the silicate melting criteria and thermal properties used in the two works. It should be noted that the planetesimal melting trend for ^{26}Al of Bizzarro et al. (2005) sharply rises above t_{onset} ~0.6 Ma. Variations in the thermal properties and the silicate melting criteria could have drastic influence on the deduced melting time in this region.

In summary, we found an excellent agreement between our results and the thermal models developed recently by Hevey and Sanders (2006). The thermal models of Ghosh and McSween (1998, 1999) and Ghosh et al. (2003) infer temperatures that are high at least by a factor of ~1.5, whereas Bizzarro et al. (2005) trends for planetesimal melting are consistent for $t_{onset} < 0.5$ Ma. In general, it is difficult to find the exact reason for the differences; however, in the case of Bizzarro et al. (2005), this could be probably due to the differences in the chosen silicate melting criteria and the thermal parameters. Finally, it should be mentioned that most of the inferences drawn from the present work are based on H-chondrite composition of the planetesimals; the thermal models developed by Bizzarro et al. (2005) and Hevey and Sanders (2006) with CI abundances would provide a complementary view of the differentiation processes in the early solar system.

Several groups in the past have used distinct ^{26}Al decay energy, namely 3 and 4 MeV for planetary heating in their thermal models. We have run simulations for a planetesimal 20 km in size with two distinct accretion scenarios and the $(^{60}Fe/^{56}Fe)_{initial}$ ratio to understand the influence of the choice of the ^{26}Al decay energy on planetary differentiation. In Table 2, the results for the two choices of ^{26}Al decay energy, i.e., 3 and 4 MeV, are compared with our choice of 3.16 MeV. Our choice is based on the total thermal energy released (Schramm et al. 1970) by the decay of ^{26}Al in the form of (1.84 MeV) γ-ray and β^+. The latter annihilates with an ambient electron to further produce two γ-rays. As neutrinos are weakly interacting particles with extremely small interaction cross section, the entire neutrino flux leaves the planetesimal carrying the entire energy produced during the electron capture and the partial energy produced during β-decay. The total thermal energy released (Schramm et al. 1970) is based on the decay scheme of ^{26}Al proposed by Ferguson (1958).

Temporal Constraints on the Accretion of the Chondrite Parent Bodies

Along with ^{26}Al, the recently revised abundance of ^{60}Fe indicates that the substantial accretion of the chondrite parent bodies should commence 2–3 Ma subsequent to the formation of the CAIs with the canonical value of ^{26}Al/^{27}Al ratio. Apart from the other simulation parameters, this time scale would critically depend upon the elemental composition of the planetesimals (Bizzarro et al. 2005; Hevey and Sanders 2006). An earlier accretion of planetesimals could have resulted in a widespread melting and differentiation of these bodies. If the two short-lived nuclei were heterogeneously distributed in the solar nebula, even an early accretion of planetesimals devoid of the two short-lived nuclides could have circumvented the intense heating and differentiation. However, the accretion of these planetesimals should occur rapidly compared to the time scales involved in the homogenization of the stellar injected short-lived nuclei in the solar nebula (Boss 2004). Since the extent of the heterogeneity of ^{26}Al in the solar nebula is estimated to be small (MacPherson et al. 1995), it is quite likely that the substantial accretion of the majority of the chondrite parent bodies were delayed in the early solar system by 2–3 Ma.

SUMMARY AND CONCLUSIONS

Detailed thermal models for the differentiation of planetesimals with mostly H-chondrite composition and undergoing accretion growth have been developed for planetesimals in the size range of 20–270 km. The models incorporate sintering at ~700 K, which leads to the compaction of the planetesimals. The dependence of the growth rate of Fe-FeS core and the extent of silicate melting on the onset time of the planetesimal accretion, the accretion duration, the final size of the body, and the (^{60}Fe/^{56}Fe)$_{\text{initial}}$ ratio has been comprehensively analyzed for two complementary differentiation scenarios. These scenarios differ in the temporal sequence of the core-mantle differentiation with respect to silicate melting and crust formation. Among the several parameters studied in the present work, the time of the initiation of core formation and the initiation of basaltic melt extrusion depends strongly on the onset time of planetesimal accretion. The other parameters begin to show their influence where the accretion starts more than 1.5 to 2 Ma after CAIs. The initiation of the accretion of the planetesimals in the solar nebula reservoir containing ^{26}Al and ^{60}Fe within the initial ~2–3 million years of the early solar system resulted in an extensive heating and differentiation. The thermal models predict the earliest Fe-FeS and basaltic melts to appear within ~0.1 million years subsequent to the onset of the accretion of the earliest planetesimals. The subsequent growth of the core depends up on the accretion duration of the planetesimal. A rapid accretion in <0.01 Ma results in almost instantaneous growth of core, whereas the accretion of a planetesimal over 1 Ma results in a slow growth of the core over couple of million years. Depending upon the accretion scenario and the initial abundances of the two short-lived nuclei, the differentiation processes in general could have continued for <10 million years. Since we could not incorporate convection in the molten mantle after the emergence of magma ocean and core-mantle differentiation, the subsequent thermal evolution of the differentiated planetesimals along with their cooling rates needs to be re-assessed.

Acknowledgments–We are extremely grateful to Drs. H. Haack, I. S. Sanders, and E. R. D. Scott for their critical comments and numerous suggestions, which led to significant improvement of our thermal models and this manuscript. We express our sincere gratitude to the reviewers for sharing their experience in thermal modeling and familiarizing us with some of the intricacies of planetary differentiation processes. This work was supported by the PLANEX grant of Indian Space Research Organization (ISRO). We are thankful to the associateship programme of Inter University Center for Astronomy and Astrophysics (IUCAA), Pune.

Editorial Handling—Dr. Edward Scott

REFERENCES

Baker J., Bizzarro M., Wittig N., Connelly J., and Haack H. 2005. Early planetesimal melting from an age of 4.5662 Gyr for differentiated meteorites. *Nature* 436:127–1131.

Bennett M. E. III and McSween H. Y., Jr. 1996. Revised model calculations for the thermal histories of ordinary chondrite parent bodies. *Meteoritics & Planetary Science* 31:783–792.

Bizzarro M., Baker J. A., and Haack H. 2004. Mg isotope evidence for contemporaneous formation of chondrules and refractory inclusions. *Nature* 431:275–278.

Bizzarro M., Baker J. A., Haack H., and Lundgaard K. L. 2005. Rapid time scales for accretion and melting of differentiated planetesimals inferred from ^{26}Al-^{26}Mg chronometry. *The Astrophysical Journal* 632:L41–44.

Bizzarro M., Ulfbeck D., and Thrane K. 2006a. Nickel isotopes in meteorites: Evidence for live ^{60}Fe and distinct ^{62}Ni isotope reservoirs in the early solar system (abstract #2020). 37th Lunar and Planetary Science Conference. CD-ROM.

Bizzarro M., Ulfbeck D., Trinquier A., Thrane K., and Connelly J. N. 2006b. Nickel isotope anomalies in meteorites (abstract). *Meteoritics & Planetary Science* 41:A21.

Boss A. P. 2004. Evolution of the solar nebula. VI. Mixing and transport of isotopic heterogeneity. *The Astrophysical Journal* 616:1265–1277.

Bottke W. F., Nesvorny D., Grimm R. E., Morbidelli A., and O'Brien D. P. 2006. Iron meteorites as remnants of planetesimals formed in the terrestrial planet region. *Nature* 439:821–824.

Chabot N. L. and Haack H. Evolution of asteroidal cores. 2006. In *Meteorites and the early solar system II*, edited by Lauretta D. S., Lesin L. A., and McSween H. Y. Jr. Tucson, Arizona: The University of Arizona Press. pp. 474–771.

Dauphas N., Foley C. N., Wadhwa M., Davis A. M., Janney P. E., Qin L., Göpel C., and Birck J.-L. 2005. Protracted core differentiation in planetesimals from ^{182}Hf-^{182}W systematics in the Eagle station pallasite (abstract #1100). 36th Lunar and Planetary Science Conference. CD-ROM.

Dodd R. T. 1981. *Meteorites: A petrologic-chemical synthesis*, 1st ed. New York: Cambridge University Press. 368 p.

Ferguson J. M. 1958. ^{26}Al decay scheme. *Physical Review* 112:1238–1240.

Ghosh A. and McSween H. Y., Jr. 1998. A thermal model for the differentiation of planetesimal 4 Vesta, based on radiogenic heating. *Icarus* 134:187–204.

Ghosh A. and McSween H. Y., Jr. 1999. Temperature dependence of specific heat capacity and its effect on planetesimal thermal models. *Meteoritics & Planetary Science* 34:121–127.

Ghosh A., Weidenschilling S. J., and McSween H. Y., Jr. 2003. Importance of the accretion process in planetesimal thermal evolution: 6 Hebe as an example. *Meteoritics & Planetary Science* 38:711–724.

Grimm R. E. and McSween H. Y., Jr. 1993. Heliocentric zoning of the planetesimal belt by aluminum-26 heating. *Science* 259:653–655.

Haack H. and McCoy T. J. 2004. Iron and stony-iron meteorites. In *Meteorites, comets and planets*, edited by Davis A. M. Treatise on Geochemistry, vol. 1, edited by Holland H. D. and Turekian K. K. Oxford: Elsevier-Pergamon. pp. 325–345.

Haack H., Baker J. A., and Bizzarro M. 2005. Accretion of differentiated planetesimals—Before, during, or after chondrule formation? (abstract) *Meteoritics & Planetary Science* 40:A62.

Hevey P. J. and Sanders S. 2006. A model for planetesimal meltdown by ^{26}Al and its implications for meteorite parent bodies. *Meteoritics & Planetary Science* 41:95–106.

Hewins R. H. and Newsom H. E. 1988. Igneous activity in the early solar system. In *Meteorites and the early solar system*, edited by Kerridge J. F. and Matthews M. S. Tucson, Arizona: The University of Arizona Press. pp. 73–101.

Horan M. F., Smoliar M. I., and Walker R. J. 1998. ^{182}W and ^{187}Re-^{187}Os systematics of iron meteorites: Chronology for melting, differentiation and crystallization in planetesimals. *Geochimica et Cosmochimica Acta* 62:545–554.

Jarosewich E. 1990. Chemical analyses of meteorites: A compilation of stony and iron meteorite analyses. *Meteoritics* 25:323–337.

Keil K. and Wilson L. 1993. Explosive volcanism and the compositions of cores of differentiated planetesimals. *Earth and Planetary Science Letters* 117:111–124.

Keil K., Stöffler D., Love S. G., and Scott E. R. D. 1997. Constraints on the role of impact heating and melting in planetesimals. *Meteoritics & Planetary Science* 32:349–363.

Kleine T., Munker C., Mezger K., and Palme H. 2002. Rapid accretion and early core formation on planetesimals and the terrestrial planets from Hf-W chronometry. *Nature* 418:952–955.

Kleine T., Mezger K., Palme H., and Scherer E. 2005a. Tungsten isotopes provide evidence that core formation in some planetesimals predates the accretion of chondrite parent bodies (abstract #1431). 36th Lunar and Planetary Science Conference. CD-ROM.

Kleine T., Mezger K., Palme H., Scherer E., and Munker C. 2005b. Early core formation in planetesimals and late accretion of chondrite parent bodies: Evidence from ^{182}Hf-^{182}W in CAIs, metal-rich chondrites, and iron meteorites. *Geochimica et Cosmochimica Acta* 69:5805–5818.

Lapidus L. and Pinder G. F. 1982. *Numerical solutions of partial differential equations in science and engineering*. New York: Wiley-Interscience Publications. 677 p.

MacPherson G. J., Davis A. M., and Zinner E. K. 1995. The distribution of aluminum-26 in the early solar system—A reappraisal. *Meteoritics* 30:365–386.

Markowski A., Quitté G., Kleine T., Bizzarro M., Leya I., Wieler R., Ammon K., and Halliday A. N. 2006. Early and rapid differentiation of planetesimals inferred from isotopic data in iron meteorites and angrites (abstract #2000). 37th Lunar and Planetary Science Conference. CD-ROM.

Marsh C. A., Della-Giustina D. N., Giacalone J., and Lauretta D. S. 2006. Experimental tests of the induction heating hypothesis for planetesimals (abstract #2078). 37th Lunar and Planetary Science Conference. CD-ROM.

McCoy T. J., Keil K., Muenow D. W., and Wilson L. 1996. Partial melting and melt migration in the acapulcoite-lodranite parent body. *Geochimica et Cosmochimica Acta* 61:637–650.

McCoy T. J., Mittlefehldt D. W., and Wilson L. 2006. Asteroid differentiation. In *Meteorites and the early solar system II*, edited by Lauretta D. S., Lesin L. A., and McSween H. Y., Jr. Tucson: The University of Arizona Press. pp. 733–745.

McSween H. Y., Jr., Ghosh A., Grimm R. E., Wilson L., and Young E. D. 2002. Thermal evolution models of planetesimal. In *Planetesimals III*, edited by Bottke W. F. Jr., Cellino A., Paolicchi P. and Binzel R. P. Tucson, Arizona: The University of Arizona Press. pp. 559–571.

Merk R., Breuer D., and Spohn T. 2002. Numerical modeling of ^{26}Al-induced radioactive melting of planetesimals considering accretion. *Icarus* 159:183–191.

Miyamoto M. 1991. Thermal metamorphism of CI and CM carbonaceous chondrites: An internal heating model. *Meteoritics* 26:111–115.

Miyamoto M., Fujii N., and Takeda H. 1981. Ordinary chondrites parent body: An internal heating model. Proceedings, 12th Lunar and Planetary Science conference. pp. 1145–1152.

Mostefaoui S., Lugmair G. W., Hoppe P., and El Goresy A. 2004. Evidence for live ^{60}Fe in meteorites. *New Astronomy Review* 48: 155–159.

Mostefaoui S., Lugmair G. W., and Hoppe P. 2005. ^{60}Fe: A heat source for planetary differentiation from a nearby supernova explosion. *The Astrophysical Journal* 625:271–277.

Nyquist L. E., Reese Y., Wiesmann H., Shih C.-Y., and Takeda H. 2001. Live ^{53}Mn and ^{26}Al in a unique cumulate eucrite with very calcic feldspar (An~98) (abstract). *Meteoritics & Planetary Science* 36:A151.

Nyquist L. E., Shih C.-Y., Wiesmann H., and Mikouchi T. 2003a. Fossil ^{26}Al and ^{53}Mn in D'Orbigny and Sahara 99555 and the time scale for angrite magmatism (abstract #1388). 34th Lunar and Planetary Science Conference. CD-ROM.

Nyquist L. E., Shih C.-Y., Wiesmann H., Yamaguchi A., and Misawa K. 2003b. Early volcanism on the NWA 011 parent body (abstract). *Meteoritics & Planetary Science* 38:A59.

Nyquist L. E., Reese Y., Wiesmann H., Shih C.-Y., and Takeda H. 2003c. Fossil ^{26}Al and ^{53}Mn in the Asuka-881394 eucrite: Evidence of the earliest crust on planetesimal 4 Vesta. *Earth and Planetary Science Letters* 214:11–25.

Qin L., Dauphas N., Wadhwa M., Janney P. E., Davis A. M., and Mazarik J. 2006. Evidence of correlated cosmogenic effects in iron meteorites: Implications for the timing of metal-silicate differentiation in planetesimals (abstract #1771). 37th Lunar and Planetary Science Conference. CD-ROM.

Sahijpal S. 1997. Isotopic studies of the early solar system objects in meteorites by an ion microprobe. Ph.D. thesis, PRL, Gujarat University, Ahmedabad, Gujarat, India.

Sahijpal S. 2006. Numerical simulations of the planetary differentiation of planetesimals (abstract #1688). 37th Lunar and Planetary Science Conference. CD-ROM.

Sahijpal S. and Soni P. 2005. Planetary differentiation of accreting planetesimals with ^{26}Al and ^{60}Fe as the heat sources (abstract #1296). 36th Lunar and Planetary Science Conference. CD-ROM.

Sahijpal S., Ivanova M. A., Kashkarov L. L., Korotkova N. N., Migdisova L. F., Nazarov M. A., and Goswami J. N. 1995. ^{26}Al as a heat source for early melting of planetesimals: Results from isotopic studies of meteorites. *Earth and Planetary Science Letters* 104:555–567.

Sanders I. S. 1996. A chondrule-forming scenario involving molten planetesimals. In *Chondrules and the protoplanetary disk*, edited by Hewins R. H., Jones R. H., and Scott E. R. D. Cambridge: Cambridge University Press. pp. 327–334.

Sanders I. S. and Taylor G. J. 2005. Implications of ^{26}Al in nebular dust: Formation of chondrules by the disruption of molten planetesimals. In *Chondrites and the protoplanetary disk*, edited by Krot A. N., Scott E. R. D., and Reipurth B. San Francisco: Astronomical Society of the Pacific. pp. 915–932.

Schramm D. N., Tera F., and Wasserburg G. J. 1970. The isotopic abundance of ^{26}Mg and limits on ^{26}Al in the early solar system. *Earth and Planetary Science Letters* 10:44–59.

Scherstén A., Elliott T., Hawkesworth C., Russell S., and Masarik J. 2006. Hf-W evidence for rapid differentiation of iron meteorite parent bodies. *Earth and Planetary Science Letters* 241:530–542.

Sonett C. P., Colburn D. S., and Schwartz K. 1968. Electrical heating of meteorite parent bodies and planets by dynamo induction from a pre-main sequence T Tauri "solar wind." *Nature* 219: 924–926.

Srinivasan G. 2002. ^{26}Al-^{26}Mg systematics in the eucrites A-881394, A-87122, and Vissannapetta (abstract). *Meteoritics & Planetary Science* 37:A135.

Srinivasan G., Goswami J. N., and Bhandari N. 1999. ^{26}Al in eucrite Piplia Kalan: Plausible heat source and formation chronology. *Science* 284:1348–1350.

Tachibana S. and Huss G. R. 2003. The initial abundance of ^{60}Fe in the solar system. *The Astrophysical Journal* 588:L41–44.

Taylor G. J. 1992. Core formation in planetesimals. *Journal of Geophysical Research* 97:14,717–14,726.

Taylor G. J., Klaus K., McCoy T. J., Haack H., and Scott E. R. D. 1993. Planetesimal differentiation: Pyroclastic volcanism to magma oceans. *Meteoritics* 28:34–52.

Urey H. C. 1955. The cosmic abundances of potassium, uranium, and thorium and the heat balances of the earth, the Moon, and Mars. *Proceedings of the National Academy of Science* 41:127–144.

Wasson J. T. and Huber H. 2006. Compositional trends among IID irons: Their possible formation from the P-rich lower magma in a two-layer core. *Geochimica et Cosmochimica Acta* 70:6153–6167.

Weidenschilling S. J. 1988. Formation processes and time scales for meteorite parent bodies. In *Meteorites and the early solar system*, edited by Kerridge J. F. and Matthews S. W. Tucson, Arizona: The University of Arizona Press. pp. 348–371.

Wood J. A. and Pellas P. 1991. What heated the parent meteorite planets? In *The sun in time*, edited by Sonnett C. P. and Giampapa M. S. Tucson, Arizona: The University of Arizona Press. pp. 740–760.

Yang J., Goldstein J. I., and Scott E. R. D. 2006. Evolution of differentiated asteroids as inferred from cooling rates of magmatic iron meteorites (abstract #5146). *Meteoritics & Planetary Science* 41:A193.

Yin Q., Jacobsen S. B., Yamashita K., Blichert-Toft J., Télouk P., and Albarède F. 2002. A short time scale for terrestrial planet formation from Hf-W chronometry of meteorites. *Nature* 418: 949–952.

Yomogida K. and Matsui T. 1983. Physical properties of ordinary chondrites. *Journal of Geophysical Research* 88:9513–9533.

Yomogida K. and Matsui T. 1984. Multiple parent bodies of ordinary chondrites. *Earth and Planetary Science Letters* 68:34–42.

Yoshino T., Walter M. J., and Katsura T. 2003. Core formation in planetesimals triggered by permeable flow. *Nature* 422:154–157.

Young E. D., Simon J. I., Galy A., Russell S. S., Tonui E., and Lovera O. 2005. Supracanonical $^{26}Al/^{27}Al$ and the residence time of CAIs in the solar protoplanetary disk. *Science* 308:223–227.